Stirring the Intracluster Medium: Heat deposition from galaxy motions

by

Aida Ghazvini Zadeh
B.Sc., K. N. Toussi University of Technology, 2004

A Thesis submitted in Partial Fulfillment of the
Requirements for the Degree of

MASTER OF SCIENCE

in the

DEPARTMENT OF PHYSICS AND ASTRONOMY

© Aida Ghazvini Zadeh, 2008
UNIVERSITY OF VICTORIA
All rights reserved. This thesis may not be reproduced in whole or in part, by photocopy or other means, without the permission of the author.

Stirring the Intracluster Medium: Heat deposition from galaxy motions

by

Aida Ghazvini Zadeh

B.Sc., K. N. Toussi University of Technology, 2004

Supervisory Committee

Dr. A. Babul, (Department of Physics and Astronomy)

Supervisor

Dr. S. Ellison, (Department of Physics and Astronomy)

Departmental Member

Dr. A. Wright, (Department of History in Art)

Outside Member

Dr. A. Mahdavi, (Department of Physics and Astronomy, San Francisco State University)

External Examiner

Supervisory Committee:

Dr. A. Babul, Supervisor (Department of Physics and Astronomy)

Dr. S. Ellison, Departmental Member (Department of Physics and Astronomy)

Dr. A. Wright, Outside Member (Department of History in Art)

Dr. A. Mahdavi, External Examiner (Department of Physics and Astronomy, San Francisco State University)

Abstract

Clusters of galaxies are the largest and most massive gravitationally bound objects in the universe. They contain several hundreds to thousands of galaxies orbiting in the gravitational potential well of the cluster. The space between galaxies is filled with a hot plasma that loses its thermal energy via X-ray emission. In the absence of heating sources in the ICM, the radiative cooling of the gas leads to a significant accumulation of cold gas in the cluster core which then should ultimately condense into stars or cold gas clouds (e.g., Fabian 1994). However, high-resolution X-ray spectroscopy of the hot intracluster gas has revealed that there is little or no signature of significant cool gas in the cluster core. This strongly suggests that there must be other forms of heating mechanisms that offset radiative losses in the intracluster medium (ICM).

In this dissertation, we focus on one of the potential heating sources in the ICM, and that involves the kinetic energy in the orbital motions of cluster galaxies. We examine in detail the effects of the heating due to dynamical friction of galaxies on the evolution of the ICM. We find that galaxy heating is immaterial in systems that are in cool core configurations with no other heating mechanisms operating in the

ICM. Accordingly, dynamical friction-mediated heating can not be the only heating mechanism in galaxy clusters. The situation is, however, completely different if the systems have experienced sufficient amounts of energy input to warm or hot cores. We show that the role of dynamical friction heating in moderating radiative cooling cannot be neglected in these systems. We also address the results of the last generation of non-radiative cosmological simulations of galaxy clusters (Voit et al. 2005). According to these studies, the radial entropy distribution of the simulated clusters tends to follow a power law at large radii, with cores present in the entropy configurations of these systems at small radii. The origin of the entropy cores is presently unclear. We argue that the generation of entropy cores in non-radiative simulated clusters is the result of galaxy stirring.

Table of Contents

List of Figures

Chapter 1 | *Introduction*

1.1 Clusters of Galaxies

A wide variety of cosmological observations support a single model for the geometry and energy content of the observable universe which is referred to as the concordance model. In this picture, the two dominant components of the total energy density of the universe are dark matter and dark energy. The dark matter accounts for approximately 25 % of the total energy density and its gravity drives structure formation in the universe. The dark energy accounts for nearly 70% of the total energy density and its negative pressure is responsible for the acceleration of the expansion of the universe at the present time (Spergel et al. 2003). Ordinary baryonic matter that comprises stars, planets, and human beings, contributes only about 4% of the total energy density of the universe and plays a minor role in the dynamics of the universe (Burles et al. 2001). Yet, it is the only component that is directly observable.

According to the concordance model, the universe, as a whole, is expanding at the present time. Gravity drives structure formation in this picture. Gravitationally bound regions decouple from the expansion. They collapse upon themselves and eventually reach a state of virial equilibrium in which the dark matter component forms stably bound halos, with the velocity dispersion providing support against gravity. Density perturbations on smaller scales have larger amplitudes in the concordance model and therefore, small objects form first and merge with other small objects to create galaxies. Galaxies merge later to create clusters of galaxies. The

formation of clusters of galaxies, therefore, directly traces the hierarchical formation of cosmic structures in the universe.

Clusters of galaxies are the largest, most massive, and most recent gravitationally bound objects in the universe with diameters of several megaparsecs (that corresponds to a few times 10^{22} meteres) and masses larger than roughly 10^{14} times that of the Sun's ($10^{14} M_{\odot}$). They contain several hundreds to thousands of galaxies orbiting in a dark matter dominated gravitational potential well. Galaxy clusters contain a very hot plasma that permeates the space between the galaxies. The intracluster gas contributes up to 90% of the total baryonic content of clusters, leaving only a small fraction of baryons locked up in stars and galaxies (Lin et al. 2003).

Clusters of galaxies provide useful tools for probing the parameters of the concordance model. For instance, they can be used to measure the total matter density of the universe, Ω_m. Galaxy clusters are very large and their potential wells are so deep that they retain all their baryons until the present time (e.g., Kay et al. 2004; Crain et al. 2006). In this respect, clusters can be thought of as "typical" regions of the universe where the ratio of their baryonic mass to total mass reaches the corresponding ratio of the universe (i.e., $M_{\rm baryons}/M_{\rm total} = \Omega_b/\Omega_m$, where Ω_b and Ω_m are the baryon density and total matter density of the universe, respectively). Thus, measurements of baryon mass fraction of galaxy clusters can be used as a probe of the universal baryon to total matter densities (e.g., White et al. 1993; Allen et al. 2002; Lin et al. 2003; Ettori 2003; Allen et al. 2004, McCarthy et al. 2007). Supplementing the baryon mass fractions with constraints on Ω_b (e.g., from cosmic microwave background measurements or a combination of Big Bang nucleosynthesis predictions and deuterium measurements from quasar absorption lines), allows us to measure the total matter density of the universe, Ω_m.

Unfortunately, it is not possible to directly observe the mass of a galaxy cluster. Instead, astronomers use baryonic observables (e.g., temperature, luminosity, velocity dispersion) as a proxy for mass. X-ray observations of clusters is used to

measure their masses through measurements of the intracluster gas temperature and density structure. The deep potential wells of clusters compress the gas and heat it to high temperatures of several keV (which corresponds to a few times 10^7 K). At these temperatures, the intracluster gas becomes fully ionized and loses thermal energy through thermal Bremsstrahlung emission (free-free emission) in the X-ray band (e.g. Sarazin 1988). One method to measure the mass of a galaxy cluster is to use the temperature and density distributions of the gas determined from X-ray observations and assume that the gas is in hydrostatic equilibrium within the gravitational potential of the cluster halo and evaluate its total mass. Optical observations of galaxy clusters also yield mass estimates through measurements of the orbital velocities of member galaxies and through measurements of the gravitational lensing of the background galaxies (e.g., Hoekstra et al. 1998; Mellier 1999).

Our understanding of galaxy clusters on both observational and theoretical fronts has advanced at a rapid pace over the past few decades. On theoretical fronts, huge progress has been achieved in the modelling of clusters of galaxies over the past few decades due to major advancements in computational methods. Numerical simulations of structure formation and evolution can now properly track the evolution of the dark matter component. These simulations, however, are not able to accurately model the evolution of the baryonic component. Modelling of the baryonic component is much more challenging than the modelling of the dark component. This is because the dark matter particles interact only through gravitational forces, whereas the baryons interact through gravitational and electromagnetic forces. Therefore, a proper model for the baryons has to take into account the effects of various non-gravitational processes on different physical length scales. An accurate modelling of the baryons is very important because they are the only particles that we can observe.

In the context of cluster observations, the advancements in technology have provided us with powerful tools to better understand the observable properties of

galaxy clusters and has led to more precise estimates of the cluster mass. The new generation of X-ray satellites, *XMM-Newton* and *Chandra*, allows us to probe the temperature and density profiles of galaxy clusters out to large radii (e.g., Pratt et al. 2006a; Sanderson et al. 2006; Vikhlinin et al. 2006; Donahue et al. 2006; Piffaretti et al. 2005; Arnaud et al. 2005). As a result, the estimates of a cluster's total mass and gas mass are substantially improved.

The extremely hot intracluster gas distorts the spectrum of the cosmic microwave background (CMB) photons by shifting them to higher energies as they pass through a cluster. This process is known as the Sunyaev-Zeldovich (SZ) effect (Sunyaev & Zeldovich 1970, 1972). Because the SZ effect is independent of redshift, the SZ effect observations can detect high redshift clusters (e.g. Carlstrom et al. 2002). Several microwave background experiments with high levels of sensitivity, including the Sunyaev-Zeldovich Array (SZA; Muchovej et al. 2006), The Atacama Cosmology Telescope (ACT; Kosowsky 2006), the South Pole Telescope (SPT; Ruhl & SPT collaboration 2004), the Arcminute Microkelvin Imager (AMI; AMI collaboration et al. 2006); the Atacama Pathfinder Experiment SZ Survey (APEX-SZ), and Planck, will yield thousands of SZ effect galaxy clusters in the next few years. The results of these experiments place tighter constraints on the parameters of the concordance model.

Major progresses have also been made in the observations of galaxy clusters in the optical band. The development of optical CCD cameras has enabled us to probe clusters through gravitational lensing of background galaxies (Hoekstra et al. 1998, 2006). Mahdavi et al. (2007) perform a joint analysis of cluster observables (JACO), which is the first method to use weak-lensing, X-ray, and SZ data simultaneously to constrain the shape of the dark matter profile in galaxy clusters.

The analyses of cluster mass estimates that involve the observed gas temperature and density profiles and assume that the gas is in hydrostatic equilibrium within the cluster's potential well are more reliable for nearby clusters that are likely to

be in equilibrium. Distant high-redshift galaxy clusters, on the other hand, are in earlier stages in their evolution and therefore, the assumptions of hydrostatic equilibrium or virial equilibrium may not be appropriate. For these systems, using the mass-observable relations (i.e., theoretical relations between a cluster's mass and its observable properties) yields more reliable estimations of the cluster mass.

Numerical simulations of galaxy clusters that only involve gravitationally-driven processes (e.g., shock heating and compression) predict self-similar relationships between various properties of clusters. These models predict the present day scaling relationship between the virial mass, X-ray gas temperature, and luminosity to follow $M \propto T^{3/2}$, and $L \propto T^2$ (Kaiser 1991; Eke et al. 1996). Observations of galaxy clusters, however, show departures from these self-similar scaling relations. Vikhlinin et al. (2006) determine the mass−temperature relation for a sample of nearby relaxed galaxy clusters and find that $M \propto T^{1.5-1.6}$ which is in agreement with the predictions of the pure gravitational models. However, there are disagreements in the normalization constants of these relations (Vikhlinin et al. 2006). On the other hand, the observed luminosity-temperature relations appear to follow $L \propto T^{2.6-2.8}$, which is steeper than the self-similar scaling. The existing discrepancies between observations and the predictions of gravitationally-driven simulations indicate that non-gravitational processes play an important role in shaping the properties of the ICM. It is therefore necessary to examine these processes and to assess their effects on the evolution of the baryonic component of galaxy clusters.

One of the most important problems regarding the properties of the cluster baryons is the so-called cooling flow problem. The extremely hot intracluster gas loses its thermal energy via Bremsstrahlung emission. Analytic calculations of the radiative losses in clusters and numerical simulations of cosmological structure formation that include radiative cooling conclude that around 30−40% of the intracluster gas must cool to form stars and cold gas clouds within the lifetime of a cluster (Balogh et al. 2001; Dave et al. 2002). However, observations of clusters

indicate that only about 9%−14% of the baryonic content of clusters reside in stars and cold molecular clouds (Lin et al. 2003). This implies that some form(s) of non-gravitational heating must counteract the radiative cooling losses of the intracluster gas. It is therefore important to quantify the associated non-gravitational heating mechanisms and incorporate them properly in the theoretical models of cluster formation and evolution. The work presented here examines one of the heating sources in the ICM, and that involves the kinetic energy in the orbital motions of cluster galaxies. The main goal of this dissertation is to study in great detail the impacts of heating due to motions of galaxies on the intracluster gas.

1.2 This Work

1.2.1 Non-Gravitational Processes in the ICM

According to recent high quality *Chandra* and *XMM-Newton* X-ray observations, clusters can be divided into three morphological classes based on the observed properties of their ICM (Poole et al. 2008). Two classes host compact cores with central temperatures that are either cool and are referred to as compact cool core (CCC) systems, or central temperatures that are warm and approximately isothermal, and are referred to as compact warm core (CWC) clusters (Donahue et al. 2005; Sanderson et al. 2006; Pratt et al. 2007). The third class hosts extended core systems with a broad range of central entropies and nearly isothermal central temperature distributions and are referred to as extended warm core (EWC) clusters. The compact core systems generally have shorter central cooling times ($\lesssim$ 2 Gyrs) comparing to extended core morphologies. The short central cooling time scale of compact core clusters implies that, in the absence of any heating sources, they will form a cooling flow leading to a significant accumulation of cold gas in the cluster core which then should ultimately condense into stars or cold gas clouds (Cowie & Binney 1977; Fabian & Nulsen 1977; Mathews & Bregman 1978; see also Fabian 1994 for

a review). However, high-resolution X-ray data from *Chandra* and *XMM-Newton* show that there is little evidence for significant cool (< 2 keV) gas in such systems (Peterson et al. 2001, 2003).

This provides a great impetus to quantify non-gravitational heating mechanisms in the ICM. Several heating mechanisms associated with different physical processes have been studied so far in the literature. One of the well studied theoretical heating models is energy injection from active galactic nuclei (AGN). As the intracluster gas loses thermal energy through X-ray emission, it sinks to the bottom of the cluster potential well. The centres of many clusters with cold gas whose cooling time is less than the age of the universe contain AGN. Post-collapse feedback from AGN in response to inflow of cooling gas is supposed to heat the ICM through the injection of relativistic jets or buoyant bubbles and suppress further accretion of gas onto the central black hole (e.g. Binney & Tabor 1995; Churazov et al. 2001; Mathews et al. 2004; Voit & Donahue 2005; Brighenti & Mathews 2006; Nusser et al. 2006; McCarthy et al. 2008). However, as discussed by McCarthy et al. (2008), the energy output from AGN activity can only explain the observed cool core clusters. The amount of energy required to drive the system from the pure cooling state to the present observed configuration is of order of $\sim 10^{62}$ ergs. The required amount of energy to transform the system into the observed range of non-cooling cores is even about an order of magnitude higher and exceeds the amount of energy that could be provided by the most powerful AGN outbursts observed to date. This fact strongly suggests that present-day AGN feedback may not be the only heating source in the ICM to supply the required energy and maintain the configuration of the system.

If the cluster gas is heated before it falls into the cluster's deep gravitational potential, the energy injection requirements to reach the present observed state would be considerably lowered (Kaiser 1991; Evrard & Henry 1991; Bower 1997; Balogh et al. 1999; Babul et al. 2002; Voit et al. 2002; Oh & Benson 2003;

McCarthy et al. 2004). The 'pre-heating' scenario (i.e., an early episode of energy injection) is much more energetically efficient than the internal heating. Pre-heated systems require up to two orders of magnitude less energy than systems that are heated internally at the present time in order to reach the observed present-day configuration (McCarthy et al. 2008). Pre-heating also seems to provide a plausible explanation for the present-day non-cooling core clusters. Clusters with higher levels of (early) energy injection will not have sufficient time to radiate this energy and therefore, the intracluster gas is still hot at the central region with long central cooling times (McCarthy et al. 2004, 2008). Pre-heating, however, appears not to be the only source of heat in cool core clusters. The relatively short central cooling times of these systems imply that some form of present-day heating process is required in the ICM. Therefore, cluster models that combine pre-heating with some form(s) of present-day heating mechanism(s) can potentially provide a better explanation for the observed structure of cool core cluster (see, e.g., McCarthy et al. 2008).

Although AGN outbursts at the centres of clusters are promising candidates for halting further condensation of the intracluster gas in cool core clusters, there are X-ray observations of clusters with short central cooling times but yet no evidence for AGN activities (Donahue et al. 2005). Donahue et al. have studied two clusters A1650 and A2244 with central cooling times of $\sim$ 1 Gyr. They find no evidence for recent episodes of AGN outbursts in these system. In the context of AGN heating scenario, these systems bring up a challenge. One possibility is that these two clusters have experienced an very strong AGN outburst $\gtrsim$ 1 Gyr in the past. Another alternative is that the central intracluster gas in these systems has never cooled to the point at which it can trigger the central black hole into action. This implies that some other heating mechanism(s) must operate in the ICM to offset radiative losses and maintain the entropy configuration of these systems.

The above issues provide strong motivations to study other potential heating

sources in the ICM that can mitigate radiative cooling losses. There is one heating mechanism that is continuously effective in the ICM but which has not received much attention and that involves the kinetic energy in the orbital motions of cluster galaxies. As a galaxy orbits in the gravitational potential well of a galaxy cluster, it deflects the background particles and generates a wake behind itself that traces its direction of motion and exerts gravitational force on the moving object. This process is called dynamical friction. The orbiting galaxies are subjected to gravitational drag from the dark matter and the hot intracluster gas particles and lose some of their dynamical energy which is then transformed into kinetic and thermal energy and deposited in the dark matter and the ICM, respectively.

Heating the intracluster gas with energy in the orbits of moving substructures has been considered on and off for nearly three decades. Schipper (1974), Lea and De Young (1976), and Raphaeli and Salpeter (1980) studied the impacts of gravitational drag on cluster gas and found that the induced heat is insufficient to forestall gas cooling. However, the inefficiency of the process as reported by these authors is because of the lower masses of the galaxies due to the absence of dark matter in their calculations. Miller (1986) showed that the generated heating due to galaxy stirring in the core of the Perseus cluster can offset radiative cooling provided the mass-to-light ratio of galaxies is about 20. El-Zant et al. (2004) revisited the above calculations using the updated galaxy and gas data for the Perseus cluster and found that for an average mass-to-light ratio of about 10, energy deposited by galaxies inside the cooling radius can counteract radiative cooling losses. Kim et al. (2005) more recently analyzed the local heating of the ICM due to dynamical friction of galaxies. They find that galaxy heating can not be the *sole* heating mechanism in the ICM; it can not, by itself, explain the observed temperature and density profiles of galaxy clusters. However, they note that galaxy stirring can be a significant source of heat in the ICM; it can mitigate radiative losses and lengthen the cooling time of the gas in the central region of clusters.

In this dissertation, we attempt to investigate in great detail the influences of galaxy heating on structural properties and thermal evolution of the intracluster gas. In order to quantify the contribution of dynamical friction of galaxies to the heating of the ICM, we develop a semi-analytical scheme for the evolution of the ICM that includes a realistic treatment of galaxy stirring heating and radiative cooling. Following the approach of Kim et al. (2005), we examine the local balance between dynamical friction-mediated heating and radiative cooling throughout the ICM. Within the context of stemming the cooling catastrophe, heating the ICM by the orbiting substructures is not expected to be dominant *in* and *of itself* (Kim et al. 2005, Conroy & Ostriker 2007). However, we show that in clusters that have evolved from a hot earlier configuration, possibly through an early episode of entropy injection, galaxy stirring has the potential to influence the thermodynamic properties of the ICM; specifically it alters the rate at which gas will cool down again. We address the observed CWC clusters by Donahue et al. (2005) and demonstrate that a cluster model that combines pre-heating, galaxy stirring heating, and radiative cooling provides a viable explanation for these systems.

Another important issue that we address is regarding the structural properties of non-radiative simulated clusters. Clusters of galaxies have been simulated for over two decades now. Has the effects of galaxy stirring been seen in these simulations? Until relatively recently, numerical simulations have not had the dynamical range to resolve more than 4−5 most massive substructures. The situation is improving, however. The latest generation of non-radiative cosmological simulations of galaxy clusters have shown that the resulting clusters have approximately self-similar radial entropy profiles (Voit et al. 2005). The radial entropy distribution tends to follow a power law at large radii. At smaller radii, there are cores present in the entropy configurations of these systems. The origin of the entropy cores is presently unclear. The flattening of the entropy profiles appears to be a physical effect and is robust to the specific technique used to carry out the simulations. We argue that the

generation of entropy cores in non-radiative simulated clusters is the result of galaxy stirring.

1.2.2 Our Semi-Analytic Approach

We study the evolution of the structural properties of galaxy clusters by modelling them semi-analytically. Specifically, we use a 1-D hydrodynamic code to track the evolution of the ICM. We neglect changes in the cluster potential and, in fact, assume that the underlying dark matter mass distribution is fixed. The model includes realistic treatment of radiative cooling and galaxy stirring heating. The main advantage of semi-analytic models is that due to their inherent simplicity, they can be easily manipulated and experimented with, leading to a wealth of information and deep physical insight about the processes that govern the formation and evolution of galaxy clusters. However, the intrinsic simplicity of our models also means that the approach has its limitations: The semi-analytic models do not fully capture the highly non-linear processes, such as the hierarchical formation of structures in the universe, and consequently, they ignore the effects of mass and substructure growth in clusters. Some additional assumptions are also usually implemented in semi-analytical models of galaxy clusters. For example, it is usually assumed that the intracluster gas is in hydrostatic equilibrium within the potential well of clusters. This assumption may not apply to clusters at high redshifts that are in earlier stages in their formation and evolution and are unlikely to be in equilibrium. Another assumption is the spherical symmetry of the system that might result in scatter in the observed properties of clusters.

For a preliminary exploration of the role of galaxy stirring, the semi-analytic approach more than suffices in terms of gaining valuable insights into (1) how these processes influence the evolution of the ICM, and (2) the competition between heating due to galaxy stirring and radiative cooling. In addition, it allows us to study the effects of pre-heating the intracluster gas on the evolution of the ICM.

The plan of the thesis is as follows. In chapter 2, we evaluate the local generated heating rate resulting from dynamical friction of the orbiting galaxies. In chapter 3, we present a detailed description of our cluster models, including the non-radiative model, the pure cooling model, and the dynamical friction heating + cooling model. We present the predictions of the models in chapters 4 and 5. Finally, we discuss our results in chapter 6 and summarize our conclusions in chapter 7. The models considered in this work are developed in a flat ΛCDM cosmology with $h = 0.7$, $\Omega_{\rm m} = 0.3$, $\Omega_\Lambda = 0.7$, and $\Omega_b = 0.02\ h^{-2}$.

Chapter 2 | *Theoretical Framework*

Dynamical friction is the process during which a massive moving object loses some of its kinetic energy due to the gravitational interactions between the object and its gravitationally induced wake. The analytical formula for the dynamical friction force on a moving object in collisionless media was first developed by Chandrasekhar (1943). He showed that as an object moves through a collisionless medium, it stirs a wake behind itself due to the deflection of the background particles. The wake exerts gravitational force on the moving object and causes it to decelerate in the direction of its motion. The Chandrasekhar dynamical friction force formula for a massive object moving through an infinite homogeneous collisionless medium with a Maxwellian distribution of particle velocities is given by

$$\mathbf{F}_{\rm DF} = -\frac{4\pi\rho G^2 M_{\rm p}^2\, I}{V^3}\mathbf{V}, \tag{2.1}$$

where $M_{\rm p}$ is the mass of the moving particle, $\mathbf{V}$ is its velocity, ρ is the density of the background medium, and I is a dimensionless coefficient defined as

$$I = \ln\left(\frac{r_{\rm max}}{r_{\rm min}}\right)\left[\mathrm{erf}\,(X) - \frac{2X}{\sqrt{\pi}}\, e^{-X^2}\right], \tag{2.2}$$

where $r_{\rm max}$ corresponds to the effective size of the surrounding medium, $r_{\rm min}$ corresponds to the effective size of the moving object, and $X = V/\left(\sqrt{2}\,\sigma\right)$, where σ is the one-dimensional velocity dispersion of the collisionless medium.

Examples of consequences of dynamical friction in astronomical systems include sinking of satellites in galaxies and orbital decay of galaxies in galaxy clusters (see,

for example, Taylor and Babul 2004, 2005a,b, Papers I, II, and III hereafter, respectively). In some cases, the surrounding background medium may be dark matter (collisionless) as well as gaseous (i.e., collisional), with pressure forces present in the latter modifying dynamical friction force exerted on the moving object. For example, galaxies orbiting around the centre of clusters stir wakes in the gaseous (colliosinal) intracluster medium (ICM). Ostriker (1999) evaluated the dynamical friction force on a massive object moving through a gaseous background medium using time-dependent linear perturbation theory. The dynamical friction force due to the gaseous component is

$$\mathbf{F}_{\rm DF} = -\frac{4\pi\rho_{\rm gas}G^2M_s^2\ I}{V^3}\mathbf{V}, \tag{2.3}$$

where M_s is the mass of the moving substructure, $\rho_{\rm gas}$ is the gas density, and the dimensionless coefficient, I, in this case is defined as

$$I \equiv \begin{cases} \frac{1}{2}\ln\left(\frac{1+\mathcal{M}}{1-\mathcal{M}}\right) - \mathcal{M}, & \mathcal{M} < 1\ , \\ \\ \frac{1}{2}\ln\left(1-\mathcal{M}^{-2}\right) + \ln\left(\frac{Vt}{r_{\rm min}}\right), & \mathcal{M} > 1\ , \end{cases} \tag{2.4}$$

In the above, $\mathcal{M} \equiv V/c_s$ is the Mach number of the motion and c_s is the local sound speed of the medium. Equation 2.3 assumes a massive object moving on a rectilinear trajectory through an infinite uniform density medium. However, numerical simulations of satellite dynamics have shown that this formula is a good approximation to the drag force on an object moving on a circular orbit through a finite medium such as the ICM (Sanchez-Salcedo & Brandenburg 1999, 2001, Kim & kim 2007), as is equation 2.1 (c.f. Paper I).

Plotted in Figure 2.1 is the gravitational drag force exerted on a massive object of mass M_s moving through a gaseous background medium of density $\rho_{\rm gas}$. The figure shows the variations of the dynamical friction force with the Mach number of the motion and the value of $\ln\left(c_{\rm s}t/r_{\rm min}\right)$. The figure also includes the dynamical

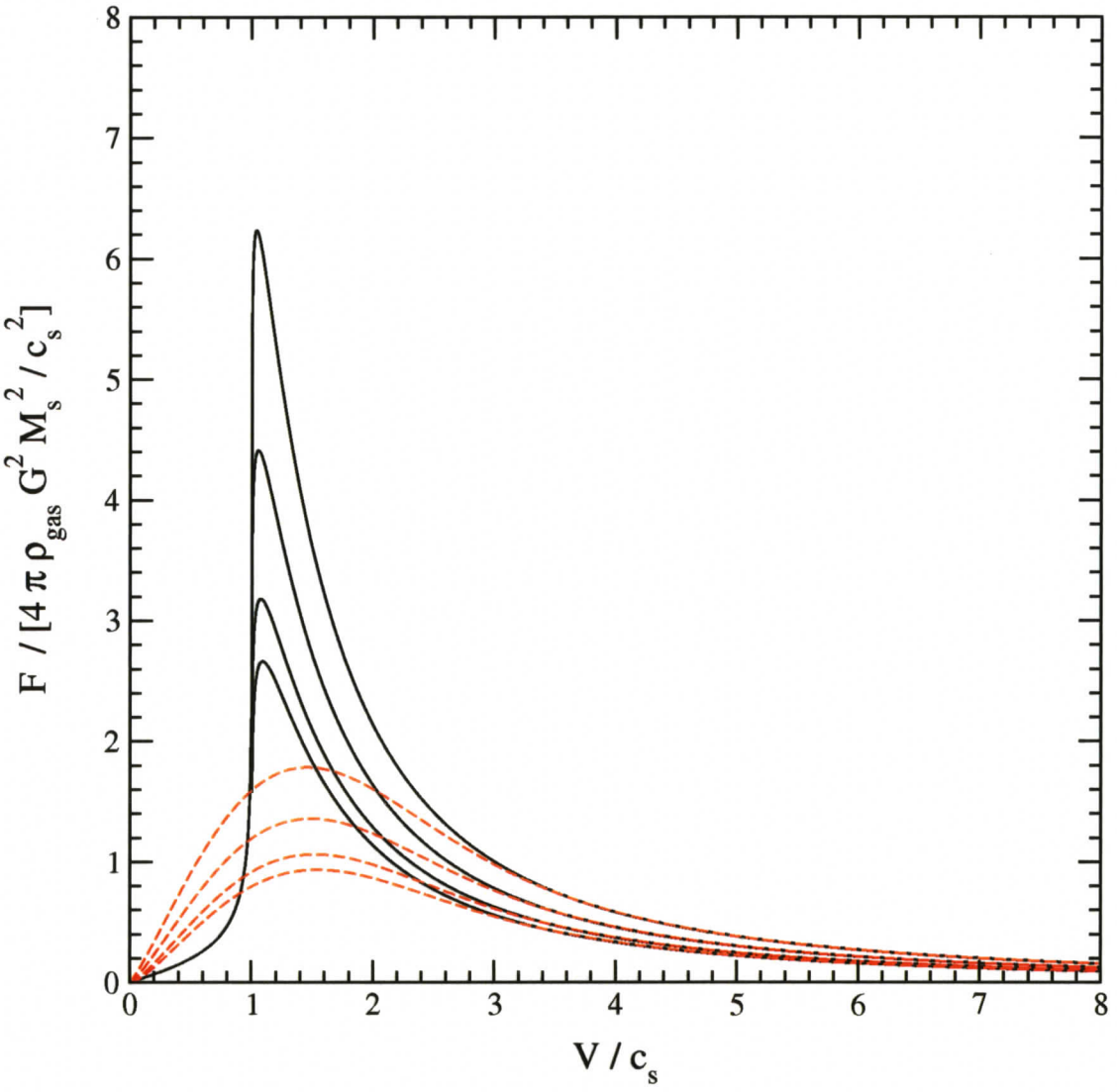

Figure 2.1: *Solid lines*- Dynamical friction force exerted on a massive object moving in a gaseous medium of density $\rho_{\rm gas}$ as a function of the Mach number of the motion, $\mathcal{M} = V/c_s$. Various curves correspond to $\ln(c_s t/r_{\rm min}) = 4$, 4.6, 6, and 8 from bottom to top (Ostriker 1999). *Dashed lines*- Dynamical friction force exerted on a particle moving in a collisionless medium of density $\rho = \rho_{\rm gas}$ and with a Maxwellian distribution of particle velocities with the velocity dispersion $\sigma = c_s$. Curves correspond to $\ln(r_{\rm max}/r_{\rm min}) = 4, 4.6, 6$, and 8 from bottom to top, and $r_{\rm max} \equiv Vt = \mathcal{M} c_s t$.

friction force on an object of the same mass moving through a medium of collisionless particles with the same density, $\rho = \rho_{\rm gas}$, and with a Maxwellian velocity distribution with $\sigma = c_{\rm s}$. Variations of the collisionless drag force with the Mach number of the object and the value of $\ln(r_{\rm max}/r_{\rm min})$ are shown in the figure. Figure 2.1 demonstrates that for subsonic motions (i.e., $\mathcal{M} < 1$), the drag force is larger in a collisionless medium than in a collisional medium. At transonic motions (i.e., $\mathcal{M} \approx 1$), which is the case for the motions of cluster galaxies with an average Much number of ~ 1.4 (e.g., Faltenbacher et al. 2005), the dynamical friction force in a gaseous medium is more sharply peaked and its value is much larger than the corresponding value in a collisionless medium. For $\mathcal{M} \gg 1$, the dynamical friction force in a gaseous medium becomes identical to the Chandrasekhar dynamical friction force formula in a collisionless medium.

The released kinetic energy due to dynamical friction of a moving satellite galaxy is converted into thermal energy of the intracluster gas via turbulent dissipation or the dissipation of resulting sound waves. The resulted heating rate per unit volume due to dynamical friction of all the orbiting galaxies is

$$\begin{aligned} < \dot{e} > &= n_s(r) \langle -\mathbf{F}_{\rm DF}.\mathbf{V} \rangle \\ &= \frac{4\pi\rho_{\rm gas} G^2 \, \langle I/\mathcal{M} \rangle}{c_s} \, \frac{n_s(r)}{N_s} \int_0^\infty M_s^2 \frac{dN}{dM_s} \, dM_s, \end{aligned} \tag{2.5}$$

where $n_s(r)$ is the radial distribution of substructure number density, N_s is the total number of substructures, M_s is the substructure mass, dN/dM_s is the differential mass function of substructures which gives the number of objects of the mass M_s to $M_s + dM_s$. The angular brackets denote an average over the velocity distribution function of substructures, $f(\mathbf{V})$, and is given by

$$\left\langle \frac{I}{\mathcal{M}} \right\rangle = \frac{\int (I/\mathcal{M}) \, f(\mathbf{V}) \, d\mathbf{V}}{\int f(\mathbf{V}) \, d\mathbf{V}}. \tag{2.6}$$

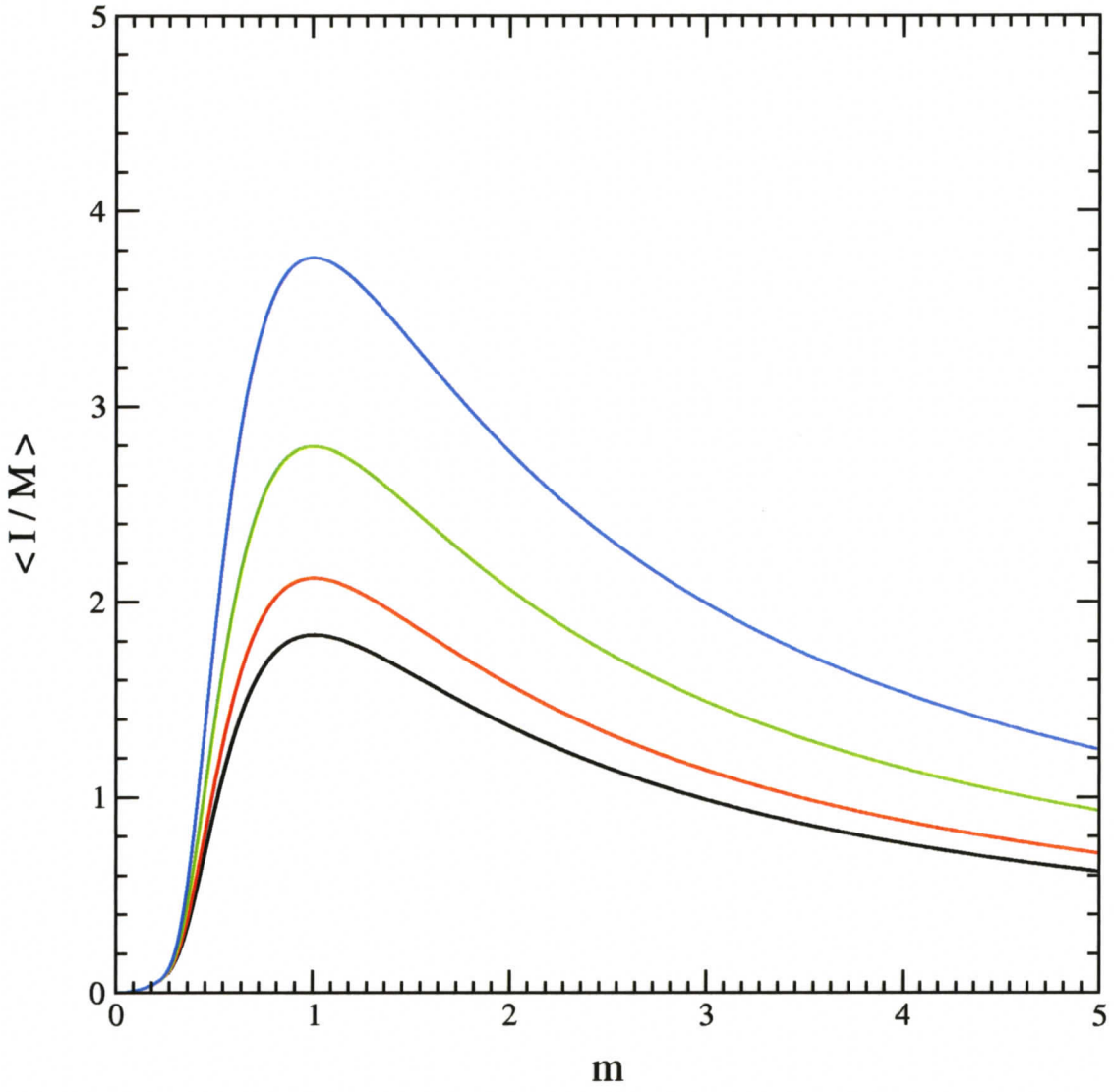

Figure 2.2: Variations of $< I/\mathcal{M} >$ as a function of $m \equiv \sigma/c_s$. The black, red, green, and blue curves correspond to $\ln(Vt/r_{\rm min})$ =4, 4.6, 6, and 8, respectively.

For simplicity, we assume that the orbital velocities of galaxies are isotropic and follow a Maxwellian distribution

$$f(\mathbf{V}) = \frac{4\pi N_s}{(2\pi\sigma_s^2)^{3/2}} V^2 e^{-V^2/(2\sigma_s^2)}, \tag{2.7}$$

where σ_s is the one-dimensional velocity dispersion of galaxies. Figure 2.2 shows how $< I/\mathcal{M} >$ varies with σ/c_s for different values of $\ln(Vt/r_{\rm min})$. We take $Vt = r_{\rm max}$ and set $r_{\rm max} \sim 1$ Mpc and $r_{\rm min} \sim 10$ kpc as the typical size of a galaxy cluster and a satellite galaxy, respectively. Therefore, $\ln(Vt/r_{\rm min}) \approx 4.6$ which corresponds to the red curve in Figure 2.2. In the remainder of this chapter we determine reasonable distributions of $n_s(r)$, dN/dM_s, and $\sigma_s(r)$, that are required in order to evaluate the heating flux (equation 2.5).

First, we quantify the radial distribution of substructure number density in galaxy clusters, $n_s(r)$, by drawing upon the semi-analytic model of satellite dynamics of Taylor & Babul (Papers II and III). Using the formalism developed in Taylor & Babul (2001), Papers II and III have examined the radial distribution of substructures in galaxy and cluster-scale halos. They find that the radial distribution of substructure number density in a typical rich cluster can be described very well by a softened (cored) form of NFW density profile

$$n_s(r) = \frac{N_0}{(r + r_{\rm core})(r + 1.15\ r_s)^2}, \tag{2.8}$$

where r_s is the scale radius of the cluster halo (see equation 2.14), $r_{\rm core} = 0.44\ r_s$ is the core radius, and n_0 is the normalization factor

$$N_0 = N_s \left(\int_0^{r_{\rm vir}} \frac{4\pi r^2}{(r + r_{\rm core})(r + 1.15\ r_s)^2}\, dr \right)^{-1}. \tag{2.9}$$

Here, $r_{\rm vir}$ is the virial radius within which the mean density of the halo exceeds the critical density, $\rho_{\rm crit(z)}$, by a factor $\Delta_{\rm crit}(z)$. For a flat ΛCDM cosmology, $\Delta_{\rm crit}(0)$ = 101.8. Plotted in Figure 2.3 is the radial distribution of substructures number

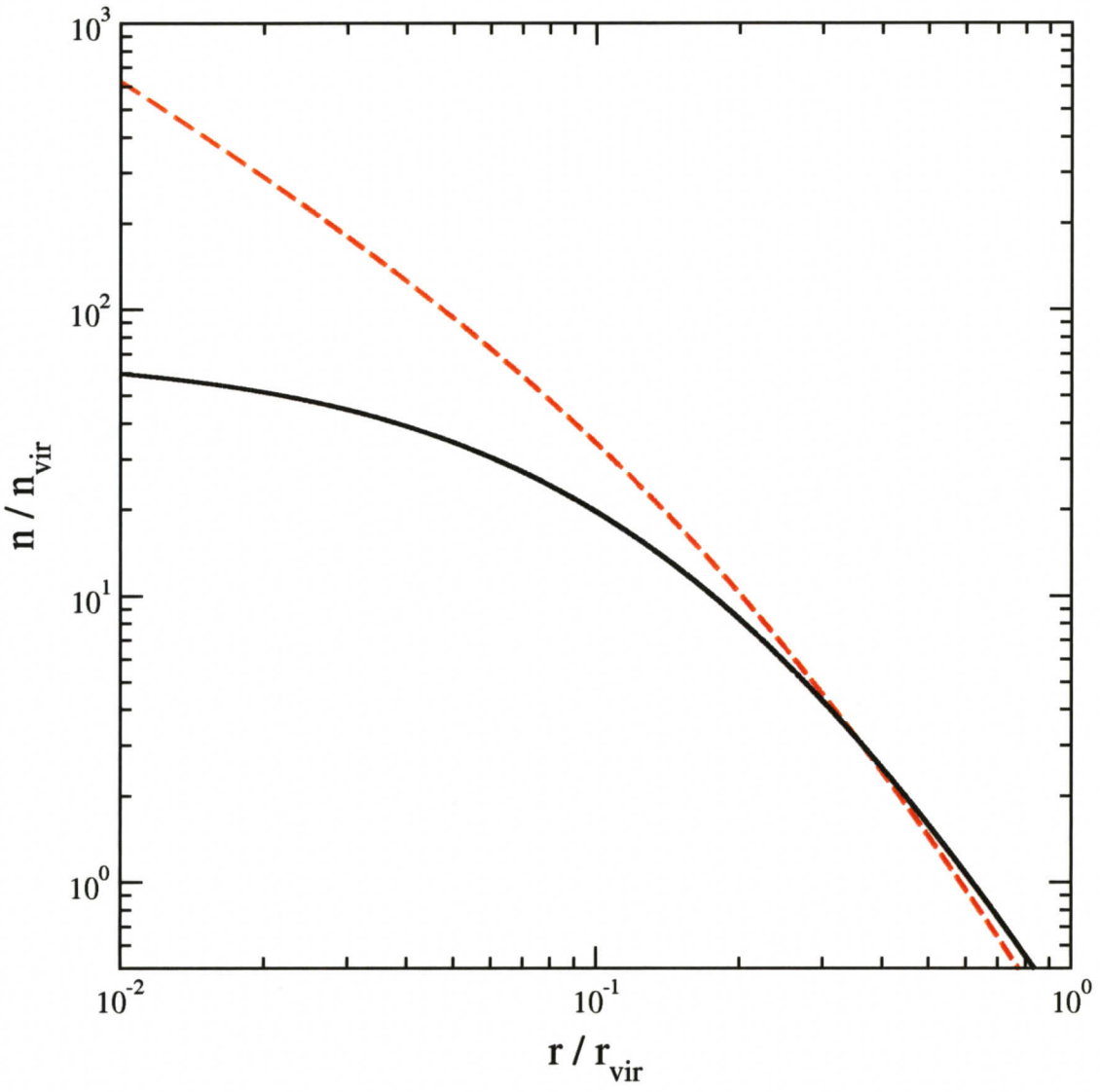

Figure 2.3: The radial distribution of substructure number density relative to the average number density of substructures within the virial radius, for a typical cluster with $M_{\rm vir} = 10^{15}\ M_{\odot}$ (Papers II and III). The dashed red line represents the density profile of the cluster halo normalized to the mean density within the virial radius.

density relative to the mean number density within the virial radius, $n_{\rm vir} \equiv N_{\rm s}/V_{\rm vir}$, for a typical rich cluster with $M_{\rm vir} = 10^{15} M_{\odot}$. The scaled density distribution of the cluster's dark halo is also shown for comparison. The total number of substructures within the virial radius, N_s, is given by

$$N_s = \int_0^{\infty} \frac{dN}{dM_s} dM_s, \tag{2.10}$$

where dN/dM_s is the differential substructure mass function. We compute the total number of galaxies by considering a reasonable galaxy mass distribution predicted by recent high-resolution numerical simulations and semi-analytical studies, as illustrated bellow.

According to the results of various numerical and semi-analytical studies, the differential subhalo mass function of a galaxy cluster halo follows a power law of the form $dN/dM_s \propto M_s^{-\alpha}$ with $1.7 \leq \alpha \leq 2.0$ (Gao et al. 2004; Kang et al. 2005; Papers II and III, Vale & Ostriker 2006), and decays exponentially in the high-mass end. Following Vale & Ostriker (2006), we adopt a Schechter-form differential mass function defined as

$$\frac{dN}{dM_s} = A_0 \Big(\frac{M_s}{M_*}\Big)^{-\alpha} \exp\Big[-\Big(\frac{M_s}{M_*}\Big)^{p}\Big], \tag{2.11}$$

where A_0 is the amplitude, α is the slope of the mass function in the low-mass regime, M_* is the cut-off mass, and p is a positive number that controls the rate of the exponential decay in the high-mass end. Spurred on by the results of various numerical studies for the substructure mass function of cluster halos in the mass range $3 \times 10^{14}\ h^{-1} M_{\odot} < M_{\rm halo} < 10^{15}\ h^{-1} M_{\odot}$ (Gao et al. 2004; Kang et al. 2005; the Millennium simulations, data kindly provided by I. McCarthy for four sample clusters; and the CLEF simulations, data kindly provided by L. Powel for three individual halos), we fit the "mean" substructure mass with the best fit parameters $A_o = 0.026$, $\alpha = 1.89$, $M_* = 0.025\ M_{\rm halo}$, and $p = 6$. We also determine the scatter in the substructure mass function. The best fit parameters to the upper

envelope are $A_0 = 0.05$, $\alpha = 1.84$, $M_* = 0.06\ M_{\rm halo}$, and $p = 6$, and the best fit parameters corresponding to the lower envelope are $A_0 = 0.014$, $\alpha = 1.94$, $M_* = 0.01\ M_{\rm halo}$, and $p = 6$. Plotted in Figure 2.4 are our fits to the differential substructure mass function against normalized mass. The solid black line represents the mean substructure mass function and the dashed green and red lines correspond to the upper and lower scatter in the mean mass function, respectively.

The last parameter that needs to be specified in order to compute the local heating rate in equation (2.5) is the velocity dispersion of cluster galaxies. We quantify the radial distribution of velocity dispersion by solving the Jeans equation

$$\frac{d\left[\sigma_s^2(r) n_s(r)\right]}{dr} = -n_s(r)\frac{d\Phi(r)}{dr}, \tag{2.12}$$

where $\Phi(r)$ is the gravitational potential of the cluster halo and $n_s(r)$ is the radial distribution of substructure number density determined in equation 2.8. To find the potential, we assume that the dark matter density distribution follows a NFW profile (Navarro et al. 1997)

$$\rho_{\rm DM}(r) = \frac{\rho_s}{(r/r_s)\left(1 + r/r_s\right)^2}, \tag{2.13}$$

where r_s is the characteristic radius and ρ_s is the characteristic density defined as

$$\rho_s = \frac{M_{200} r_s^{-3}}{4\pi\left[\ln\left(1 + c_{200}\right) - c_{200}/\left(1 + c_{200}\right)\right]}. \tag{2.14}$$

In the above, $c_{200} \equiv r_{200}/r_s$ is the concentration parameter, r_{200} is the radius within which the mean density is 200 times the critical density, $\rho_{\rm crit}(z)$, and $M_{200} \equiv M(r_{200}) = (4/3)\pi r^3{}_{200} \times 200\ \rho_{\rm crit}(z)$. For a typical massive cluster with $M_{200} = 10^{15}\ M_\odot$, r_{200} is ~ 2 Mpc. We adopt the mass-concentration relation resulted from recent cosmological simulations (Springel et al. 2005). According to this relation, the concentration parameter of a massive cluster with $M_{200} = 10^{15}\ M_\odot$ has a value

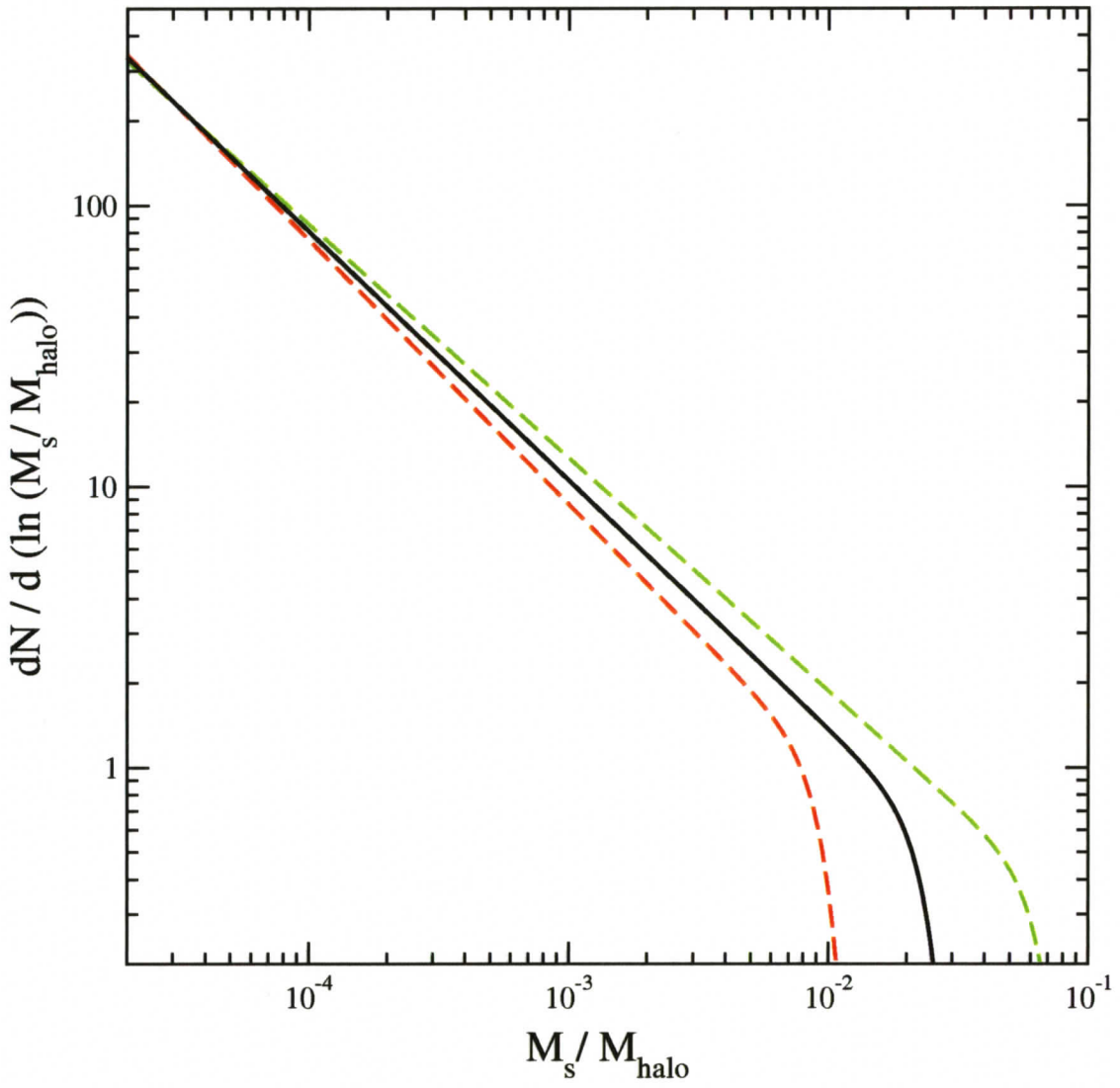

Figure 2.4: Differential subhalo mass function as a function of scaled substructure mass, $M_s/M_{\rm halo}$, for clusters in the mass range $3\times10^{14}\ h^{-1}M_\odot < M_s < 10^{15}\ h^{-1}M_\odot$. The black solid line represents the mean differential substructure mass function and the dashed red and green lines correspond to the lower and upper scatter in the mass function, respectively.

of ≈ 4.3 (Neto et al. 2007). Using equations (2.13) and (2.14) we can evaluate the gravitational acceleration

$$-\frac{d\Phi}{dr} = -4\pi G\rho_s r_s \left[\frac{\ln(1+r/r_s)}{(r/r_s)^2} - \frac{1}{(r/r_s)(1+r/r_s)}\right], \tag{2.15}$$

and solve the Jeans equation for $\sigma_s(r)$.

Equations (2.8), (2.11), and (2.12) completely specify the local heating rate per unit volume throughout the cluster halo (equation 2.5). The induced heating due to galaxy stirring is expected to be deposited throughout the galactic wake. Unfortunately, the functional form of the energy distribution through galactic wakes is unknown due to the poorly understood characteristics of the ICM turbulence. We assume throughout this work that heat is deposited locally at the position of each galaxy. However, Kim et al. (2005) examined the effects of distributed heating by adopting Gaussian and logarithmic heat distribution functions. They found that the results are qualitatively similar to the results of the model that assumes localized heating.

It should be noted that there is another mechanism which leads to the generation of wakes behind the orbiting satellites, and that is the hydrodynamic interactions between the ICM and the interstellar medium (ISM) in galaxies. During such interactions, interstellar gas will be stripped when the dynamic pressure is sufficiently strong to overcome the gravitational force which binds the gas to the galaxy. This results in prolonged tails of gas moving behind the orbiting satellites. We expect that most of the gas in the galaxies will be removed soon after the galaxies first fall into the cluster. For the purpose of this study, we will therefore neglect hydrodynamic interactions and focus on gravitationally induced wakes that are formed due to the deflection of gas and dark matter particles by the gravity of galaxies (Bondi & Hoyle 1944). The deposited energy in the ICM due to ram pressure stripping of the satellites is in addition to the dynamical friction-induced heating.

In the next chapter, we describe our cluster model and discuss the implementa-

tion of dynamical friction-mediated heating.

Chapter 3 | *Cluster Model*

The main goal of this thesis is to study how the dynamical friction-induced heating mitigates the radiative cooling losses of the intracluster gas and shapes the properties of the ICM. We examine the role of pre-heating in this picture and study how an early episode of entropy injection modifies the evolution of the ICM. To do this, we use a time-dependent one-dimensional hydrodynamic code developed by McCarthy et al. (2004) to model the cluster and track the impact of various physical processes. The simulation code provides a realistic treatment of radiative cooling and is designed to take into account the effects of pre-heating of the ICM. We expand the model to include the heating generated by dynamical friction of a cluster's substructures throughout the cluster halo. This chapter starts with a discussion of the initial setup of the dark and gaseous baryonic components of the model cluster. We will then describe the treatment of radiative cooling and dynamical friction heating that govern the evolution of the system.

3.1 The Baseline Model

The dark halo of our model clusters is filled with hot diffuse gas that is in hydrostatic equilibrium with cluster's gravitational potential, which is dominated by dark matter. We assume that the cluster potential is static. This assumption is motivated by the results of cosmological simulations that indicate that a large fraction of the mass of a rich cluster halo has been assembled more than approximately 5 Gyrs in the past (Cohn & White 2005). The gravitational potential of the cluster may be deepened if a large amount of baryons cool and sink to the bottom of the

potential as the cluster evolves. However, recent high-resolution X-ray observations of galaxy clusters have shown that the gas cooling is happening, but at a much reduced rate than derived from pure radiative cooling considerations (Peterson et al. 2003), an interpretation that is also supported by a recent optical study that finds active star formation in centrally located BCGs in cool core clusters but at much reduced rates (Bildfell et al. 2008). Accordingly, we neglect the effects of cold baryons on the potential well of our model clusters.

We determine the initial entropy configuration of the gas based on the results of recent non-radiative cosmological simulations (Voit et al. 2005). According to these simulations, the entropy profiles of non-radiative clusters are self-similar at large radii and follow a power law

$$\frac{S(r)}{S_{200}} = 1.47\Big(\frac{r}{r_{200}}\Big)^{1.22}, \tag{3.1}$$

where S is the proxy quantity that represents the gas entropy and is defined as $S = k_{\rm B}T/n_e^{2/3}$, where n_e is the electron number density and $k_{\rm B}$ is the Boltzmann's constant *. In the above, S_{200} is the characteristic entropy and is defined as

$$S_{200} = \frac{k_{\rm B}T_{200}}{[n_{e,200}]^{2/3}}, \tag{3.2}$$

where $T_{200} \equiv GM_{200}\mu m_p/2r_{200}$ is the characteristic temperature and $n_{e,200} \equiv 200\ f_b\rho_{crit}(z)/(\mu_e m_p)$ is the mean electron number density inside r_{200} assuming that the ratio of electrons to dark matter remains constant. We assume that the metallicity of the gas is $Z = 0.3Z_\odot$. The corresponding values of the mean molecular weight and mean molecular weight per free electron of the intracluster gas with this metallicity are $\mu = 0.59$ and $\mu_e = 1.14$, respectively. At the redshift of $z = 0$, the value of the characteristic entropy is given by McCarthy et al. (2008) as

*The entropy, S, is related to the thermodynamic specific entropy ,s, by $ds \propto \ln dS^{3/2}$.

$$S_{200} = 2561 \text{ keV cm}^2 \left(\frac{M_{200}}{10^{15}\ M_\odot}\right)^{2/3} \left(\frac{h}{0.7}\ \frac{f_b}{0.13}\right)^{-2/3}, \tag{3.3}$$

where $f_b \equiv \Omega_b/\Omega_m$ is the universal baryon fraction.

At smaller radii ($r \lesssim 0.1\ r_{200}$), there are cores present in the baseline entropy profiles of the simulated non-radiative clusters. The origin of this entropy core is presently unclear. We hypothesize that the core is due to heating associated with galaxy stirring. In order to test this hypothesis, we consider the evolution of the intracluster model in the absence of radiative cooling. Consequently, the evolution of the ICM, once the cluster has formed and the system has settled into equilibrium, is governed solely by the heating associated with dynamical friction of the orbiting satellites. We start by assuming that the initial entropy profile is a pure power law (equation 3.1) at all radii. We find that galaxy heating is not only able to generate cores but also the range of core entropy values observed in the cosmological simulations of Voit et al. (2005).

Having established the dark matter density distribution and the initial gas entropy profile of the baseline cluster model, we determine other properties of the intracluster gas such as its temperature, density, and pressure, by assuming that the gas is in hydrostatic equilibrium within the gravitational potential well of the cluster and solving the equation of hydrostatic equilibrium

$$\frac{dP\,(r)}{dr} = -\frac{GM_{\mathrm{DM}(r)}\ \rho_{\mathrm{gas}}\,(r)}{r^2}. \tag{3.4}$$

As for the boundary condition of the differential equation, we assume that

$$\frac{M_{\mathrm{gas}}\,(r_{200})}{M_{200}} = f_b. \tag{3.5}$$

This assumption is motivated by the results of cosmological simulations of clusters that indicate that the ratio of the gas mass to the total mass of a cluster approximately approaches the universal ratio, f_b, at the cluster periphery (Frenk et al.

1999, Kay et al. 2004). By determining the remaining gas parameters, we have completely specified the properties of the baseline gravitational model. Thereafter, we subject the baseline model to radiative cooling and dynamical friction heating and assess the effects of these processes on the evolution of the intracluster gas.

3.2 The Implementation of Radiative Cooling and Galaxy Heating

As described by McCarthy et al. (2004; 2008), the baseline dark matter and gas profiles are mapped on to a discrete non-uniform grid that has a higher resolution at the central region of the model cluster, where the impacts of radiative cooling losses and dynamical friction-mediated heating are more pronounced. The simulation evolves with time following the effects of cooling and galaxy stirring heating. We track the evolution of the entropy profile of the intracluster gas rather then the gas density and temperature individually because under the assumption of hydrostatic equilibrium, both the gas density and temperature profiles can be derived from the entropy profile. The entropy of the gas increases when heat energy is deposited in the ICM and decreases when the gas loses its thermal energy. The variation in the entropy of a parcel of gas due to the effects of radiative cooling and dynamical friction heating is given by

$$\frac{d \ln S^{3/2}}{dt} = \frac{\mu m_p \Gamma_{tot}}{\rho_{\rm gas} k_B T}, \tag{3.6}$$

where $\Gamma_{\rm tot} \equiv \Gamma_{\rm cool} + \Gamma_{\rm DF}$ is the total rate of thermal energy exchange per unit volume. Here, $\Gamma_{\rm cool}$ is the rate of energy loss per unit volume due to radiative cooling of the intracluster gas and $\Gamma_{\rm DF}$ is the rate of energy deposition per unit volume due to dynamical friction of the cluster galaxies. The cooling rate per unit volume is given by

$$\Gamma_{\rm cool} = -n_H n_e \Lambda\left(T\right), \tag{3.7}$$

where $\Lambda\left(T\right)$ is the cooling function which is calculated using a Raymond-Smith model (Raymond & Smith, 1977) with a metallicity of $Z = 0.3\ Z_{\odot}$. The local heating rate per unit volume due to dynamical friction was derived in § 2 and is given by

$$\begin{aligned} \Gamma_{\rm DF} &= < \dot{e} > \\ &= \frac{4\pi\rho_{\rm gas} G^2 < I/\mathcal{M} >}{c_s} \frac{n_s(r)}{N_{\rm vir}} \int_0^{\infty} M_s^2 \frac{dN}{dM_s}\ dM_s. \end{aligned} \tag{3.8}$$

Note that $\Gamma_{\rm cool}$ scales as ${\rho^2}_{\rm gas}$ while $\Gamma_{\rm DF}$ scales as $\rho_{\rm gas}$. This implies that cooling is more efficient in cool over-dense regions and less efficient in under-dense media.

We determine the new entropy configuration of the gas after a short time interval, dt, by integrating equation 3.6 (McCarthy et al. 2004). The size of the time interval is chosen to be less than the minimum value of $\Delta r/c_s$ computed for all gas mass shells, where Δr is the thickness of a shell. Assuming that the potential is static and that the gas pressure does not change over the small time step, dt, other properties of the ICM are evaluated by placing the gas in hydrostatic equilibrium within the potential well of the cluster and solving the differential equations of hydrostatic equilibrium

$$\frac{dP}{dM_{\rm gas}} = -\frac{GM_{\rm DM}}{4\pi r^4}, \tag{3.9}$$

and mass continuity

$$\frac{dM_{\rm gas}}{dr} = 4\pi r^2 \rho_{\rm gas}. \tag{3.10}$$

We assume the following boundary conditions to recompute the hydrostatic equilibrium:

$$\begin{aligned} r(0) &= 0, \\ r(M_{\rm gas,tot}) &= r_{\rm end}, \\ P(M_{\rm gas,tot}) &= \left[P_{200}^{2/5} + \frac{2}{5K_{200}^{3/5}} \int_{r_{\rm end}}^{r_{200}} \frac{GM_{\rm DM}(r)}{r^2}\, dr\right]. \end{aligned} \tag{3.11}$$

According to the last boundary condition, we assume that the outermost gas mass shell is compressed or expanded adiabatically. The two-point boundary value problem with the eigenvalue of $r_{\rm end}$ is solved using a relaxation technique.

The model cluster is evolved forward with time following the effects of galaxy stirring heating and radiative cooling. If the radiative cooling exceeds the dynamical friction heating (or if we consider a pure cooling cluster model that neglects galaxy heating), the temperature of the gas at the centre will eventually approach zero and it will drop out of the X-ray emitting phase. Within the context of our cluster model, we assume that if the temperature of a parcel of gas falls below $\approx 10^5\ K$, or if its entropy falls to zero, the gas drops out and turns into cold gas clouds or stars. In this case, the time steps are chosen to be sufficiently small so that only a few gas shells drop out at each time interval. As the gas cools, a flow of cooling gas will be established in the ICM. As a result, the outer gas mass shells with higher pressure flow inward and replace the cool gas that just dropped out. The model cluster is then placed back in hydrostatic equilibrium and other gas properties such as its density, temperature, and pressure are updated. In the next two chapters, we present the results of our models and discuss the consequences of non-gravitational processes on the evolution of the ICM.

Chapter 4

The Effects of Radiative Cooling and Dynamical Friction Heating

In this chapter the impacts of radiative cooling and dynamical friction-mediated heating on the evolution of the ICM are examined. We first consider non-radiative model clusters and argue that dynamical friction of substructures is responsible for the flattening of the entropy profiles inside the cluster core observed in cosmological simulations of Voit et al. (2005). Next, we examine the pure cooling model that neglects the effects of dynamical friction heating in the ICM. We use the pure cooling model as a baseline to assess the impacts of dynamical friction heating on the ICM. In the last section of this chapter, we explore model clusters where both the effects of radiative cooling of the diffuse gas and dynamical friction heating are included. We study the evolution of the ICM in clusters that have experienced different levels of initial entropy injection, focusing on the competition between cooling and galaxy heating.

4.1 Non-radiative Cluster Model

Clusters that form and evolve without losing their thermal energy through X-ray emission are unphysical systems. However, they constitute an important baseline against which to determine the impacts of radiative cooling and non-gravitational heating processes on the evolution of the ICM (c.f. Lewis et al. 2000). Cosmological

simulations of purely gravitational cluster formation determine the baseline entropy profiles of galaxy clusters in the absence of non-gravitational processes (Voit et al. 2005). The results of these simulations indicate that the radial entropy profiles of the hot intracluster gas is self similar (i.e., the radial distribution is independent of the cluster mass) and tends to follow a power law ($S(r) \propto r^{1.2}$) at large radii, as first noted by Lewis et al. (2000). Within the cluster core ($r \lesssim 0.1 r_{200}$), the profiles flatten to form a near-isentropic core, with a large distribution in the value of the central entropy. The observed flattening of the entropy profiles inside this radius is believed to be a real physical effect since over the years, the degree of flattening has been shown not to depend on the resolution of the simulations or on the specific technique used to carry out the simulations. However, the origin of the entropy cores is not yet understood. We address this issue in the context of a non-radiative cluster model. In the absence of radiative cooling, galaxy stirring heating is the only heating mechanism that can influence the ICM. Hence, the the evolution of the entropy profiles of the non-radiative clusters demonstrates the efficacy of dynamical friction-induced heating.

We adopt an initial entropy profile that follows the self-similar gravitational profile (equation 3.1) at all radii. A typical cluster with $M_{200} = 10^{15}\ M_{\odot}$ is considered. This value lies in the mass range of the simulated non-radiative clusters of Voit et al. (2005).

Plotted in Figure 4.1 are the entropy profile predictions of the non-radiative cluster model after $t = 5$ Gyrs, which is comparable to the typical age of present-day massive clusters. The entropy profiles are normalized to the characteristic entropy of the cluster, S_{200}, which has a value of ≈ 2561 keV cm^2 for our sample model cluster (equation ??). The solid red curve corresponds to the mean substructure mass function that we determined in Figure 2.4. The green and blue solid curves correspond to the lower and upper scatter in the mass function, respectively, and the dashed magenta line shows the initial entropy distribution of the system. The

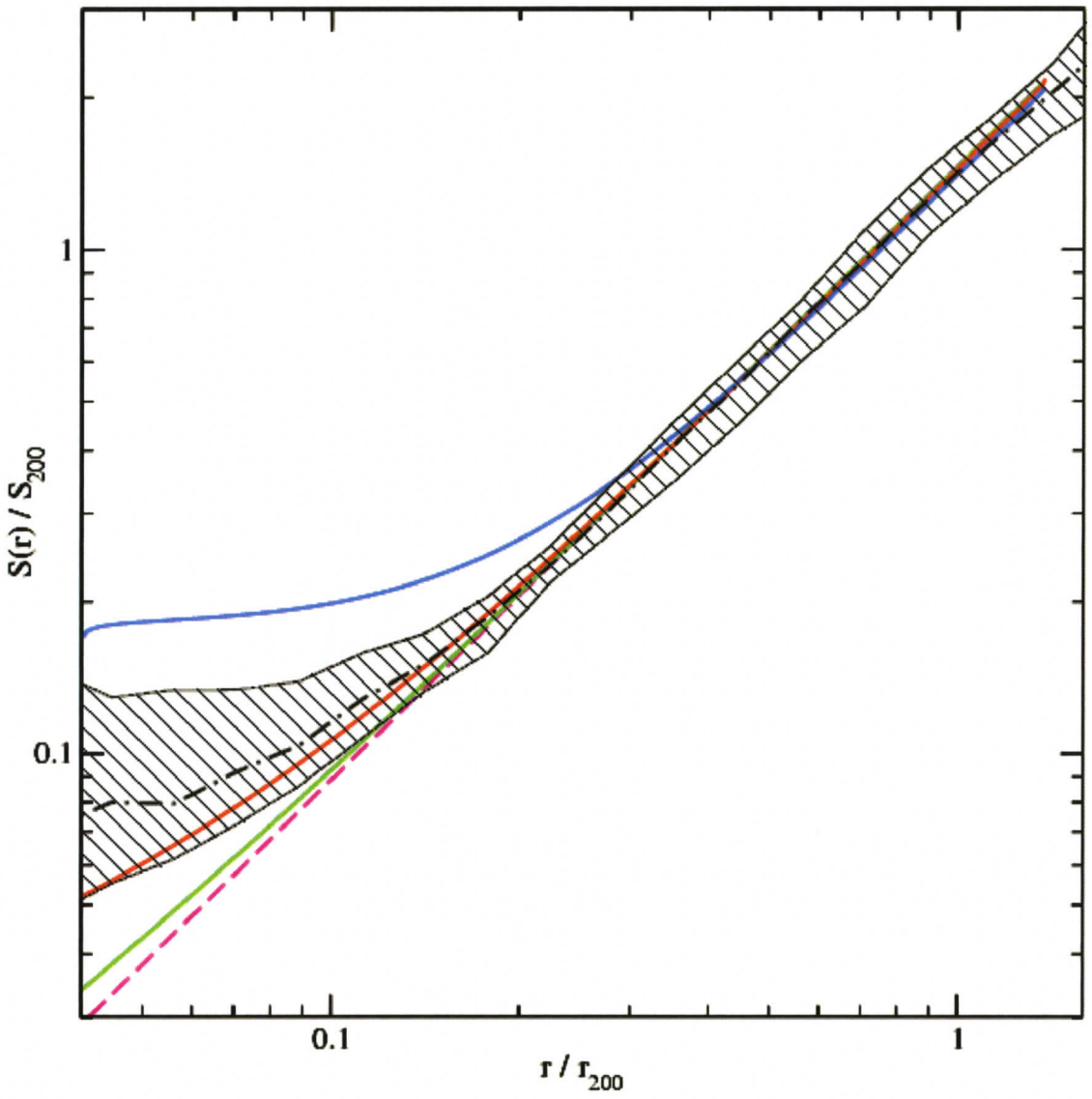

Figure 4.1: Dimensionless entropy as a function of scale radius, r/r_{200}, predicted by the non-radiative model for a typical cluster with $M_{200} = 10^{15}\ M_{\odot}$ at $t = 5$ Gyrs. The characteristic entropy of the system, S_{200}, has a value of ≈ 2561 keV cm^2. The solid red curve corresponds to the model cluster with the mean substructure mass function. The blue and green curves correspond to the upper and lower scatter in the mass function (Figure 2.4). The dashed magenta line shows the initial entropy configuration of the system. The shaded region represents the entropy profiles of the simulated non-radiative clusters of Voit et al. (2005) and the dot-dashed black curve is their median entropy profile.

shaded region represents the entropy profiles of the simulated clusters of Voit et al. (2005) and the dot-dashed black curve is their median entropy profile. As the figure indicates, the entropy profiles of our non-radiative model clusters do not change beyond the radius $r \gtrsim 0.2\ r_{200}$ and trace out the initial power law. This is because the heating flux due to dynamical friction scales linearly with the gas density and number density of substructures. Since these two parameters have higher values at the cluster centre and drop outside the cluster core, we expect dynamical friction heating to be preferentially occurring at the centre.

Inside the cluster core, however, there is more diversity in the final configuration of the cluster entropy. The flattening of the entropy profiles and the distribution of the core entropies of our non-radiative model clusters are in excellent agreement with the results of the non-radiative cosmological simulations of Voit et al. (2005). Since dynamical friction heating scales with the substructure mass as M_s^2, low-mass substructures would not contribute considerably to the heating of the intracluster gas. Therefore, clusters with a larger abundance of low-mass subhalos are not influenced by galaxy heating and the entropy profiles of these systems do not evolve appreciably with time (the lower green curve in Figure 4.1). On the other hand, dynamical friction heating is most efficient in halos with a large abundance of massive substructures. The upper blue curve in Figure 4.1 corresponds to a sample cluster with a large population of massive subhalos that are continuously present in the ICM as the system evolves with time. Dynamical friction of these massive objects contributes to an enormous amount of heating in the ICM and the central entropy of the system exceeds the highest value of the central entropy of the simulated clusters of Voit et al. (2005). The central entropies of model clusters whose substructure mass functions lie between the mean mass function and its upper scatter cover the range of entropy floors predicted by simulations.

4.2 Pure Cooling Model

Realistic clusters are not non-radiative. The hot intracluster gas loses its thermal energy prolifically through X-ray emission. In the absence of any heating sources in the ICM, the gas continues to cool until it drops out of the X-ray emitting phase as its entropy approaches zero. This happens preferentially at cluster centres where the gas is the densest and consequently, the radiative losses are maximal.

The pure cooling model, wherein only radiative losses are taken into account, constitutes a baseline against which to examine the impacts of the dynamical friction-induced heating on the evolution of the ICM. We assume that the initial gas entropy profile follows the self-similar gravitational entropy profile (equation 3.1) outside of the cluster core and flattens at small radii to form isentropic cores. This is the general form of the entropy profile of clusters as determined by *XMM-Newton* and *Chandra* observations (Donahue et al. 2006; Vikhlinin et al. 2006; Pratt et al. 2006; see also Figure 1 of McCarthy et al. 2008 that shows the distribution of central entropy in real clusters). The value of the entropy core is left as a free parameter in this model and we consider clusters with various levels of entropy injection.

Figure 4.2 demonstrates the evolution of the entropy profiles in the pure cooling model for a model cluster with $M_{200} = 10^{15}\ M_{\odot}$ for 5 Gyrs, which is comparable to the age of the present-day clusters. The various panels correspond to different values of the initial core entropy. In all cases, the baseline entropy profile is generally unchanged at large radii ($r \gtrsim 0.2r_{200}$). This is because the cooling time of the gas in this region is long relative to the age of the system. At small radii, the evolution depends sensitively on the core entropy value, as discussed in depth by McCarthy et al. (2004).

The top two panels of Figure 4.2 show that clusters with low initial central entropies ($S_o = 10$ keV cm^2 and 30 keV cm^2) start cooling out their entropy core on a relatively short timescale. The entropy core steepens as the intracluster gas

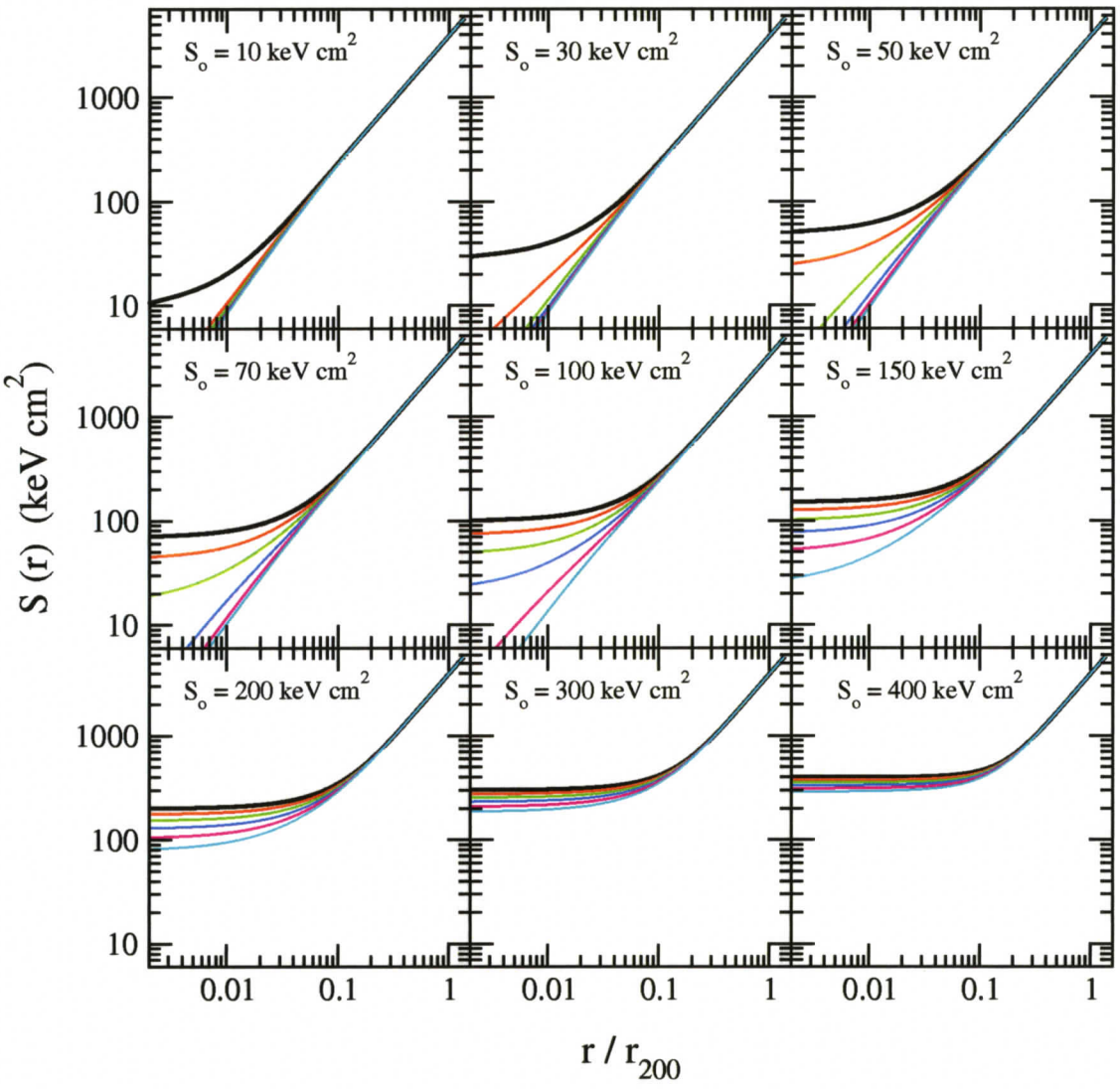

Figure 4.2: Evolution of the entropy profiles predicted by the pure cooling model for a typical cluster with $M_{200} = 10^{15}\ M_{\odot}$. The different panels correspond to various levels of the core entropy. The solid black lines represent the initial entropy configuration. The red, green, blue, magenta, and cyan curves represent the entropy distribution after 1, 2, 3, 4, and 5 Gyrs of evolution, respectively.

cools. This continues until the elevated entropy at the center completely cools out and a pure power law ($S(r) \propto r^{1.22}$) remains extending throughout the cluster halo. At this time, the cluster reaches a quasi-steady state and the power law entropy profile is maintained at all radii. This leads to the accumulation of significant amount of cooled gas in the cluster core.

Increasing the level of core entropy to S_o = 50 keV cm^2– 70 keV cm^2 slightly delays the gas drop out but does not prevent the formation of massive cooling flow towards the centre of the cluster. For S_o = 100 keV cm^2, the development of a cooling flow is delayed further; however, after approximately 5 Gyrs of radiative cooling, the cooling flow is established. Increasing the level of the central entropy to S_o = 150 keV cm^2 and higher leads delays of longer than 5 Gyrs. For instance, for an injection level of S_o = 200keV cm^2, the central entropy of the gas only drops to approximately 80 keV cm^2 after cooling for 5 Gyrs. At higher levels ($S_o \gtrsim$ 200 keV cm^2), the cooling timescale approaches the Hubble time.

Our cooling model predicts that all clusters will ultimately reach a quasi-steady state that is characterized by a pure power law entropy distribution that extends from the cluster centre to its periphery. The time needed by a cluster to reach this state, however, depends sensitively on the value of the initial core entropy once the cluster has relaxed into hydrostatic equilibrium.

Observations of clusters indicate that real clusters exhibit a broad range of central entropy distributions. The short central cooling times of the observed cool core clusters imply that the radiative cooling of the gas would rapidly lead to the overabundance of cooled material in the cluster core. However, recent high-resolution observations of galaxy clusters have demonstrated that there is no signature of significant gas cooling below a few keV in present-day cool core clusters (Peterson et al. 2003). Therefore, the central core of these systems are warmer than the pure cooling considerations. This strongly suggests that in addition to initial entropy injection, some form of present-day heating mechanism must be present in cool core

clusters. In the next section, we embed dynamical friction heating within our model clusters. We examine how dynamical friction heating influences the evolution of the ICM.

4.3 Cluster Model with Heating and Cooling

In this section, we consider a model that takes into account the effects of cooling of the gas and dynamical friction of the galaxies. Similar to the pure cooling model, we assume that the initial entropy profile follows the gravitational profile outside of the cluster core and flattens at small radii to form isentropic cores. The substructure mass function is assumed to be static and to follow the mean substructure mass function in Figure 2.4.

Figure 4.3 shows the entropy profile predictions of the dynamical friction heating + cooling model for a typical rich cluster with $M_{200} = 10^{15}\ M_{\odot}$. The upper left two panels correspond to clusters with relatively low core entropies: $S_o = 10$ keV cm^2 and 30 keV cm^2. As the Figure shows, the clusters start cooling out their entropy cores in less than 1 Gyr. A comparison of these results to those predicted by the pure cooling model (Figure 4.2) demonstrates that dynamical friction heating is immaterial in cool core clusters. This is because radiative cooling scales as the gas density squared, while dynamical friction heating scales linearly with the density. Hence radiative losses are dominant at cool over-dense cluster centre and galaxy heating cannot remedy the overcooling problem.

Increasing the level of the core entropy to $S_o = 50$ keV cm^2– 70 keV cm^2 results in an improvement relative to the pure cooling model. The cooling model predicts that a cooling flow develops in clusters with an initial central floor of S_o = 50 keV cm^2 and 70 keV cm^2 after approximately 2 and 3 Gyrs of evolution, respectively. However, according to the results of the dynamical friction heating + cooling model, clusters with an initial central entropy of $S_o = 50$ keV cm^2 start

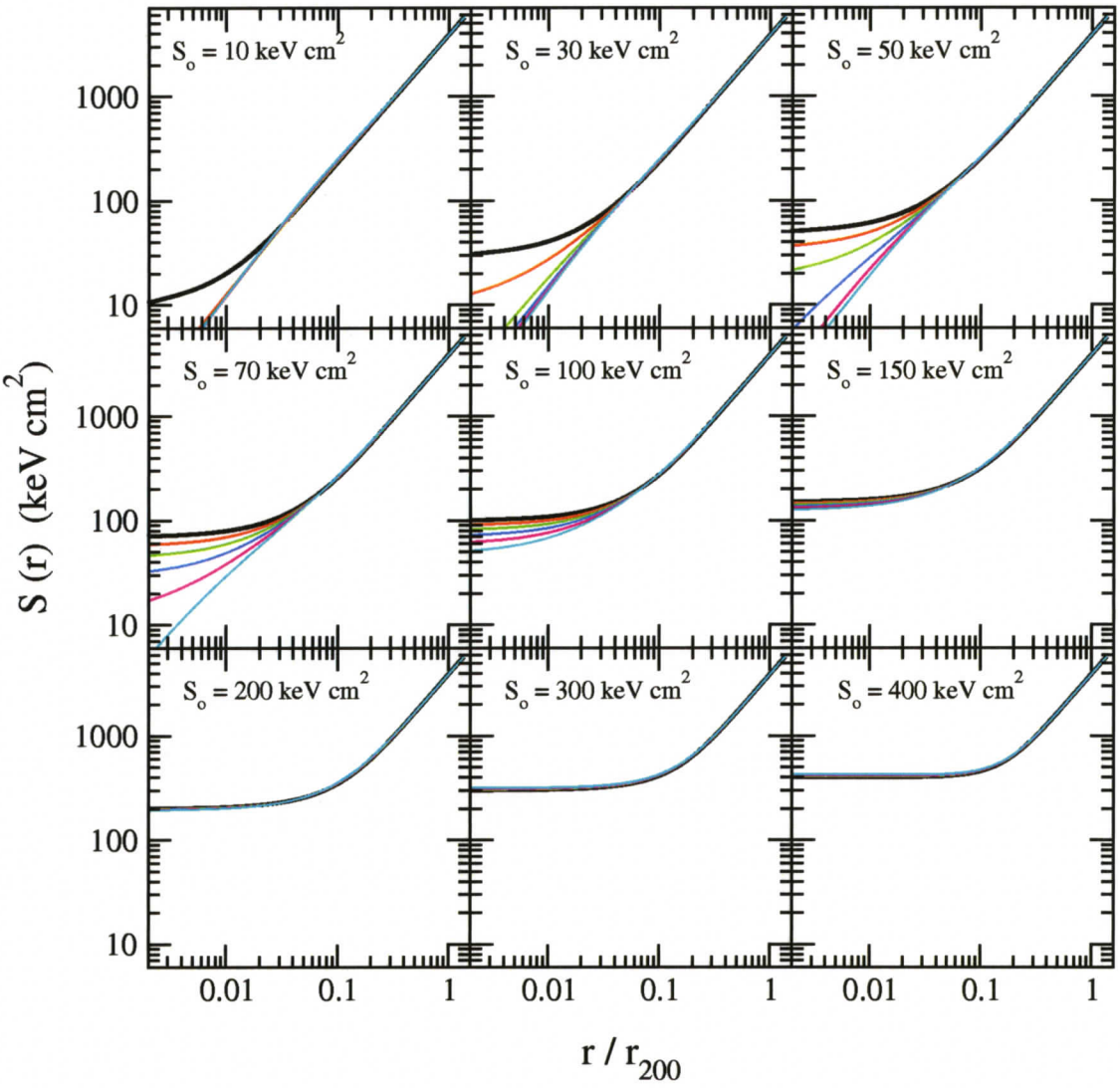

Figure 4.3: Evolution of the entropy profile predicted by the dynamical friction heating + cooling model for a typical cluster with $M_{200} = 10^{15}\ M_{\odot}$. The different panels correspond to the various levels of the core entropy. The solid black lines represent the initial entropy configuration. The red, green, blue, magenta, and cyan lines represent the entropy distribution after 1, 2, 3, 4, and 5 Gyrs of evolution, respectively.

cooling out the gas after evolving for nearly 4 Gyrs and the value of the central entropy in clusters with $S_o = 70$ keV cm^2 drops to approximately 5 keV cm^2 after ~ 5 Gyrs. As a result of galaxy stirring-heating, the cooling time of the gas in the central regions of the model clusters with mildly enhanced levels of core entropies, $S_o = 50$ keV cm^2– 70 keV cm^2, increases and the development of the cooling flow is significantly delayed. This is because radiative cooling is less efficient in these warm core systems with lower densities compared to cool core systems wherein the radiative losses are maximal. Although galaxy stirring delays the onset of cooling catastrophe in this case, it is unable to completely forestall radiative cooling of the gas inside the cluster core.

As the level of the initial entropy floor increases, radiative losses become even less efficient and the mitigating effect of dynamical friction heating becomes significantly more apparent. In systems with core entropy values of $S_o = 100$ keV cm^2, the central entropy of the model cluster only declines to approximately 50 keV cm^2 after nearly 5 Gyrs of evolution, whereas in the corresponding pure cooling case, the cooling flow is established after nearly 4 Gyrs. In the presence of an initial entropy floor of $S_o = 150$ keV cm^2– 500 keV cm^2, the dynamical friction-mediated heating can completely counteract radiative losses of the gas in the central regions of clusters and maintain the entropy core. According to the predictions of the pure cooling model, the entropy change of the central gas is very little for initial core entropy values of $S_o \geq 300$ keV cm^2. However, the entropy threshold is lower by a factor of ~ 2 in the presence of galaxy stirring heating due to the efficiency of dynamical friction of satellite galaxies in warm under-dense regions.

The results presented thus far correspond to a model cluster with a substructure mass function that follows the mean mass function fitted in §2 (Figure 2.4). As noted earlier, dynamical friction heating scales as the square of substructure mass, $M_s{}^2$, and consequently, massive objects contribute more to the heating of the intracluster gas. Therefore, we expect that galaxy heating is much more efficient in systems

with a larger population of massive substructures (i.e., shallower substructure mass function) and that the induced heating is able to offset the radiative losses with central entropies lower than $S_o = 150$ keV cm^2, as noted above where we focused on the mean substructure mass function. Figure 4.4 plots the cumulative substructure mass function which gives the total number of subhalos with masses larger than M_s. The solid black line and the dashed blue lines correspond to our fits to the mean substructure mass function and the scatter in the mass function, respectively (§2.4). The solid red curve represents a mass function with $A_o = 0.035$, $\alpha = 1.86$, $M_* = 0.04\ M_{\rm halo}$, and $p = 6$ (equation 2.11). Figure 4.5 presents the evolution of the entropy profile in a cluster whose cumulative mass function follows the red curve in Figure 4.4. The cluster has a typical mass of $M_{200} = 10^{15}\ M_\odot$. As the figure indicates, galaxy stirring heating can balance radiative losses of the central gas in this systems even if the central entropy is as low as $S_o = 50$ keV cm^2.

Based on the above results we conclude that if the system starts out in a cool core configuration, heating by dynamical friction of satellite galaxies has virtually no effect. However, the outcome is very different if the cluster has experienced sufficient amount of entropy injection to warm or hot cores. The role of dynamical friction heating in moderating radiative cooling cannot be neglected if the systems have enhanced central entropies. This provides a viable explanation for the observed configuration of CWC clusters. Donahue et al. (2005) study *Chandra* observations of two clusters with short central cooling times yet no evidence for recent AGN activities. The two clusters Abell 1650 and Abell 2244 have central entropy levels of 30 keV cm^2 and 50 keV cm^2, respectively, which is markedly higher than in clusters with more prominent radio emission (Donahue et al. 2006). These two systems have a central cooling time of ~ 1 Gyr which is longer than clusters that show evidence for AGN feedback and have central cooling times of ~ 0.1 Gyr. One possible interpretation is that these systems have experienced a powerful AGN outburst that happened $\gtrsim 1$ Gyr in the past. In the context of the galaxy heating

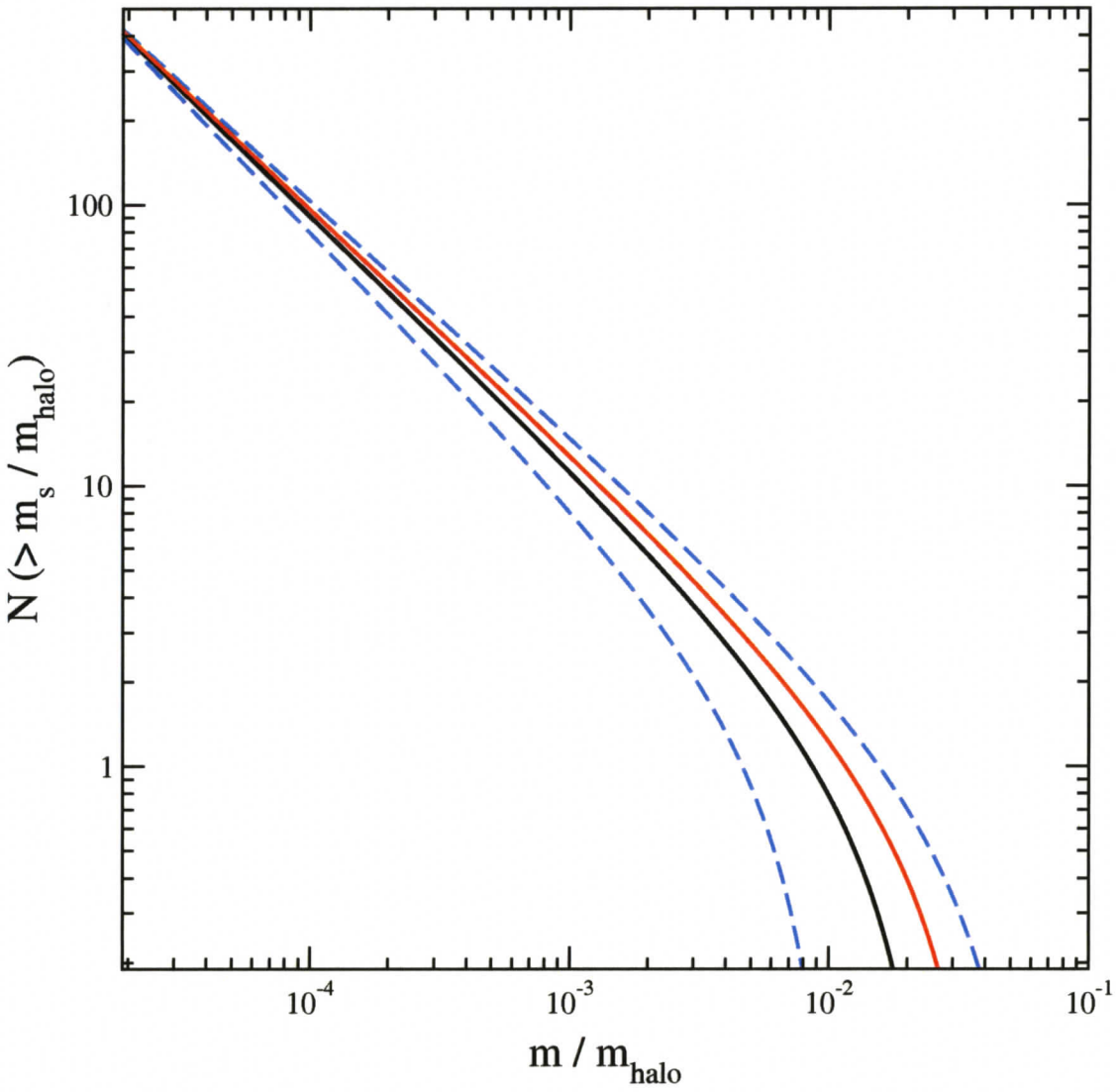

Figure 4.4: Cumulative substructure mass function as a function of the scaled substructure mass, $M_s/M_{\rm halo}$, for clusters in the mass range $3 \times 10^{14} - 10^{15}\ h^{-1}M_\odot$. The solid black curve represents the mean substructure mass function. The dashed blue lines correspond to the scatter in the mass function. The red curve represents a cumulative mass function for which the dynamical friction heating can offset the radiative losses of the gas in the presence of an initial entropy floor of $S_o = 50$ keV cm^2 for a cluster with $M_{200} = 10^{15} M_\odot$.

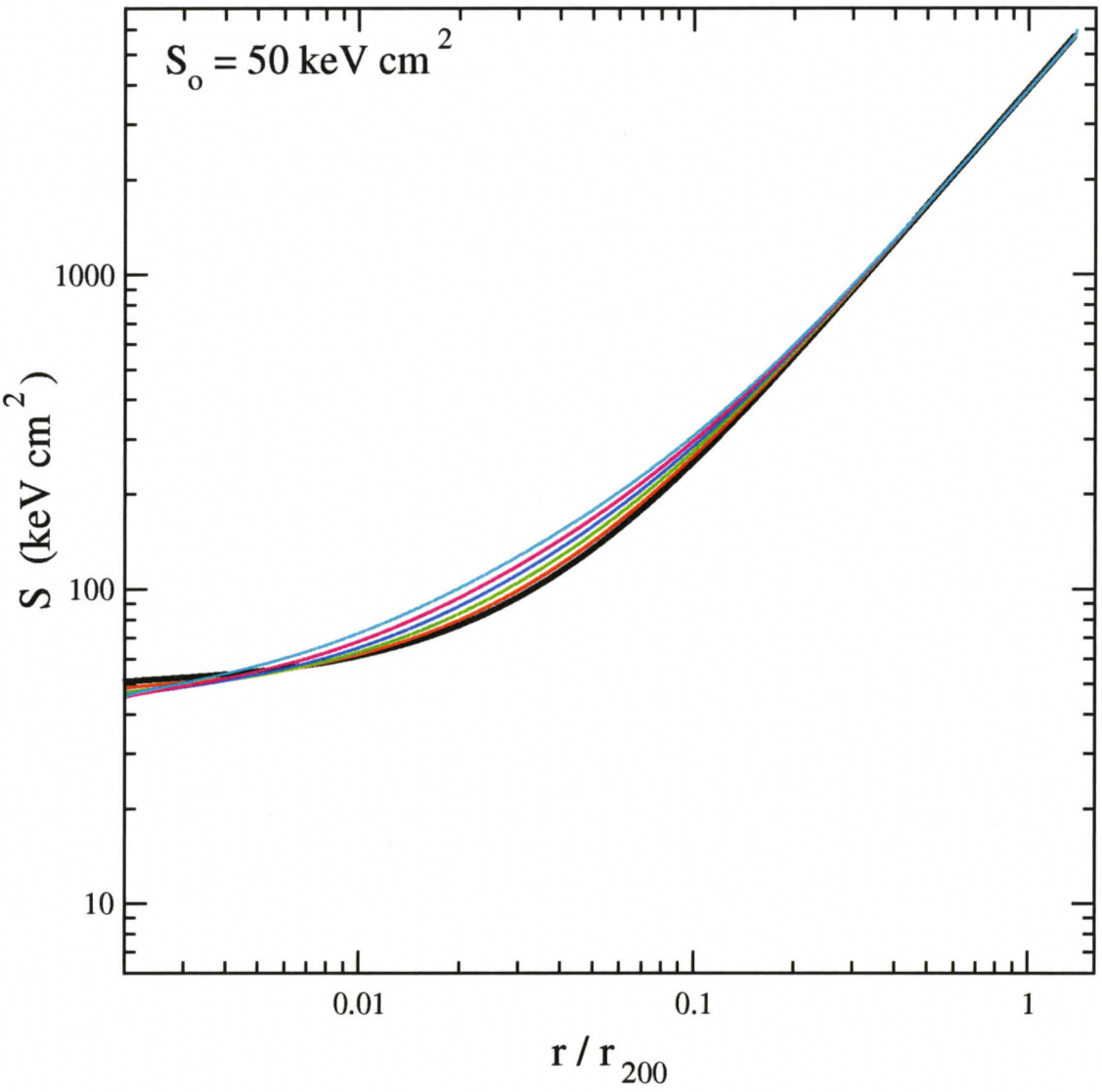

Figure 4.5: Evolution of the entropy profiles for a cluster with a typical mass $M_{200} = 10^{15}\ M_{\odot}$. The cumulative substructure mass function of the cluster follows the red curve in Figure 4.4. The black solid curve represents the initial entropy profile. The red, green, blue, magenta, and cyan lines correspond to entropy distributions after 1, 2, 3, 4, and 5 Gyrs of evolution, respectively. In the presence of a mild level of core entropy of $S_o = 50$ keV cm^2, dynamical friction-mediated heating can balance radiative cooling losses in the central region of the cluster.

model, since dynamical friction of galaxies can lengthen the cooling time of the gas in warm environments, the AGN outburst could have happened at an earlier time in these systems. The pure cooling model predicts that the central entropies of systems with $S_o = 55$ keV cm^2 and $S_o = 75$ keV cm^2 drop to 30 keV cm^2 and 50 keV cm^2, respectively, after evolving for 1 Gyr (Figure 4.2). In the presence of galaxy stirring-heating the cooling time of the gas is significantly lengthened such that the central entropies of sample clusters with $S_o = 55$ keV cm^2 and $S_o = 70$ keV cm^2 reach 30 keV cm^2 and 50 keV cm^2, respectively, after approximately 2 Gyrs of radiative cooling (Figure 4.3). This implies that the two observed clusters, Abell 1650 and Abell 2244, may have experienced a strong AGN outburst $\gtrsim 2$ Gyrs in the past.

Another interpretation is that the central gas in these two clusters has never cooled to the point at which it can trigger an AGN feedback. In this context, it is possible that the systems have experienced early episodes of entropy injection possibly before the epoch of cluster formation (e.g. McCarthy et al. 2004, 2008). According to pure cooling considerations, central entropies of clusters with $S_o =$ 150 keV cm^2 and 180 keV cm^2 drop to approximately 30 keV cm^2 and 50 keV cm^2, respectively, after cooling for 5 Gyrs, which is comparable to the typical age of present-day massive clusters. The required levels of initial entropy injection is substantially lowered in the presence of galaxy stirring-heating. Based on Figure 4.3, initial core entropies of 85 keV cm^2 and 100 keV cm^2 are sufficient to reach central entropies of 30 keV cm^2 and 50 keV cm^2 after about 5 Gyrs of radiative cooling. The value of the initial central entropy can be even reduced to $S_o \sim 50$ keV cm^2 in systems with a large population of massive substructures (Figure 4.5). We will discuss the structural properties of the observed warm core clusters and the possible interpretations of such systems in more detail in § 6.

Subhalos lose mass by tidal stripping and gravitational shocks as they orbit inside the main halo (Paper I). The more massive systems, as a result of being

subjected to greater dynamical friction, will tend to sink towards the halo centre and get disrupted. Since galaxy heating depends sensitively on these more massive substructures, one could argue that we are overestimating the heating by assuming a static subhalo mass function. In addition, one can note that we use a late-time ($z = 0$) substructure mass function at all times. However, at earlier epochs, we expect there have been many more massive subhalos as the cluster is being assembled. Also, merging inherent in the hierarchical model for structure formation will replenish subhalos. The true evolution of the substructure mass function is the product of these competing effects. In the next section, we present a simple model to examine the effects of the variations of the subhalo mass function on the evolution of the gas entropy.

Chapter 5

The Evolution of the Substructure Mass Function

In the previous chapter we developed a simple cluster model that takes into account the effects of dynamical friction heating caused by the motions of the orbiting satellites. It was assumed for simplicity that the subhalo mass function does not evolve with time. In realistic systems, however, the substructure mass function evolves according to the mass-accretion history of the halo. A proper model for the evolution of the substructure mass function of a sample cluster halo requires the incorporation of merger tree algorithms and detailed analysis of the dynamical evolution of individual substructures as they orbit within the potential of the parent halo (Paper I). This is beyond the scope of the present study. Here we try to develop a simple approach to model the evolution of the substructure mass function by drawing upon the semi-analytic model of halo formation of Benson et al. (2002a,b, 2003). We use a sample of 20 realizations of the merger tree algorithm of Benson et al., which was kindly provided by A. J. Benson, for an individual cluster halo with $M_{200} \sim 10^{15}\ M_{\odot}$. Each realization contains several time-steps over a span of ~ 5 Gyrs.

The results of the merger tree realizations suggest that cluster models with evolving substructure mass functions can be classified into two types. The first type corresponds to clusters that are in a merger phase and are gaining mass and the second type corresponds to clusters that are in a post-merger phase where the

injection of substructures has tapered off. Since the evolution of the substructure mass function of the two types of models is completely different, we will consider the two cases separately in this chapter. It should be noted that the scheme presented in this chapter does not follow the dynamical evolution of individual satellites in the cluster halo and therefore does not accurately calculate the variations of the substructure mass function. However, it provides a qualitative evaluation of the evolution of the mass function and its effects on the induced dynamical friction heating. Our goal is to study how efficiently the induced heat due to dynamical friction of the satellite galaxies affects the thermal evolution of the ICM.

5.1 Clusters in Merger Phase

Drawing upon the semi-analytic formalism of halo formation of Benson et al., we develop a simple model for the evolution of the mass function in systems that are in merger phase. We find that for 15 clusters in our sample of 20 realizations of the merger tree, the variations of the mass function are stochastic and do not follow a specific evolutionary trend. This is due to the stochastic process of merging. Once merged, objects orbit in the cluster halo and experience mass loss through tidal stripping and gravitational shocks (Paper I). The substructure mass function steepens due to the mass loss of massive satellites. As more massive objects further merge with the cluster halo, the substructure mass function becomes shallower again (Paper III). The slope of the mass function depends on the masses of the merged satellites. Accordingly, the merger frequency and the orbital decay of the merged satellites and other cluster members govern the evolution of the substructure mass function.

Plotting the entire spread in the mass functions at different time steps, we find that the mean mass function and the upper and lower limits of its scatter are in agreement with those determined in the static case in §2 (Figure 2.4). We find

that the slope of the substructure mass function in the power law regime, α, varies stochastically on time intervals of ~ 0.25 Gyr. The variations of α could be very well modeled with a Gaussian distribution with a dispersion of $\sigma_\alpha = 0.02$

$$f(\alpha) = \frac{1}{\sigma_\alpha \sqrt{2\pi}} e^{-(\alpha-\alpha_m)^2/(2\sigma_\alpha^2)}. \tag{5.1}$$

The mean slope of the mass function, α_m, varies from one cluster to another but its value lies within the range $1.7 \leq \alpha \leq 2.0$, which is in agreement with the results of other numerical and semi-analytic studies (Gao et al. 2004; Kang et al. 2005; Paper II and III).

The amplitude of the cumulative substructure mass function is roughly fixed at $M_s/M_{\rm halo} = 10^{-5}$ and its value is ≈ 700. This is in accordance with our fits to the static mass functions in Figure 4.4. We use this condition to set the amplitude of the differential substructure mass function, A_0 (equation 2.11). The mass function follows a pure power law ($dN/dM_s \propto {M_s}^{-\alpha}$) in the low-mass regime. Therefore, knowing the slope of the mass function and the total number of subhalos more massive than a mass threshold, we can integrate the differential substructure mass function and compute the amplitude at each time step.

According to equation 2.11, there are two more parameters needed to be specified in order to fully determine the differential substructure mass function at each time step; the cutoff mass, M_*, and the constant power of the exponential part, p. We fix the value of p to $p = 6$ as we did in §2. This ensures that the subhalo mass function drops properly at the high mass end. The value of slope of the mass function, α, and the cutoff mass, M_*, are correlated. We see the general trend that systems with a steeper mass function and a lower abundance of massive substructures have lower values of M_*, and clusters with a shallower mass functions and a larger population of massive objects have larger values of M_*. For the purpose at hand, we use the set of 20 semi-analytic realizations to guide us in defining a simple but reasonable relationship between α and M_*. We leave the accurate modeling of the evolution

of the mass function for future work.

We assume that the cutoff mass corresponding to the mean slope of the substructure mass function in the stochastic model, α_m, is equal to the cutoff mass of the mean mass function in the static model, i.e., $M_* = 0.025$ (§ 2). We then take the cutoff mass corresponding to the steepest and shallowest mass functions in the stochastic model (with slopes of $\alpha_{\rm sh}$ and $\alpha_{\rm st}$, respectively) to be equal to the cutoff mass of the lower and upper scatter of the mass function in the static model (i.e., $M_{*,\rm st} = 0.01$ for the lower scatter and $M_{*,\rm sh} = 0.06$ for the upper scatter). Accordingly, the range of the variations of the cutoff mass is chosen to be the same in both static and stochastic models, $0.01 \leq M_* \leq 0.06$. So far we have specified the cutoff mass corresponding to the highest, mean, and lowest slope of the randomly evolving mass functions. For intermediate values of the slope, we assume a linear correlation between α and M_* in their ranges of variation

$$M_* \approx \begin{cases} 0.025 - \frac{\alpha_m - \alpha_{\rm sh}}{0.035}\,(\alpha - \alpha_m), & \alpha_m < \alpha < \alpha_{\rm sh}\ , \\ \\ 0.025 - \frac{\alpha_m - \alpha_{\rm st}}{0.015}\,(\alpha_m - \alpha), & \alpha_{\rm st} < \alpha < \alpha_m\ . \end{cases} \tag{5.2}$$

To summarize, the amplitude of the mass function, A_o, the low-mass-end slope, α, the cutoff mass, M_*, and the power of the exponential term, p, are the four parameters that we determined above to fully specify the substructure mass function.

We first consider a model with a mean slope of $\alpha_{m,A} = 1.89$, which is the same as the slope of the mean mass function in the static model. The corresponding M_* to the mean slope and the low-mass-end amplitude, A_0, are also the same as that of the static mean mass function by definition. Accordingly, for the choice of $\alpha_{m,A}$ we can qualitatively compare the results of the two models. We refer to this model here as model A. The typical variations of the slope lie in the range $1.84 \lesssim \alpha \lesssim 1.94$ for this model.

As mentioned earlier, the mean slope of the substructure mass function varies

from one cluster to another. Accordingly, we consider two more cluster models with $\alpha_{m,B} = 1.84$ and $\alpha_{m,C} = 1.94$, and we refer to them as model B and model C, respectively. The values of $\alpha_{m,B}$ and $\alpha_{m,C}$ are chosen to be equal to the slopes of the higher and lower scatter in the mean substructure mass function in the static cluster model, respectively (§ 2). This is because, in addition to studying the effects of slope variations on dynamical friction-induced heating, the chosen values of α_m enable us to qualitatively compare the results of the non-radiative cluster models with static and stochactically evolving mass functions, as will be illustrated in §5.1.1. The variations of the slope of the mass function lie in the range $1.79 \lesssim \alpha \lesssim 1.89$ for model B and $1.89 \lesssim \alpha \lesssim 1.99$ for model C.

The remainder of this section presents the predictions of cluster models with randomly evolving substructure mass functions. We first discuss the results of non-radiative cluster models in §5.1.1. Next, we consider model clusters with radiative cooling in §5.1.2 and examine the influences of dynamical friction-mediated heating on the evolution of the ICM.

5.1.1 Non-Radiative Cluster Model

The initial set up of the three non-radiative cluster models with stochastically evolving substructure mass functions are the same and are exactly similar to that of the non-radiative static model (§ 4.1), with the initial entropy distribution following a power law of $S(r) \propto r^{1.2}$ throughout the cluster halo. Figure 5.1 presents the results of the models for sample clusters with $M_{200} = 10^{15}\ M_{\odot}$. The three red, green, and blue curves represent the entropy predictions of models A, B, and C, respectively, after evolving for 5 Gyrs, which is comparable to the age of the present-day clusters. The dashed magenta line is the initial entropy profile. The shaded region represents the scatter in the entropy profiles of the non-radiative simulated clusters of Voit et al. (2005, see their Figure 1) and the dot-dashed black curve corresponds to their median entropy distribution.

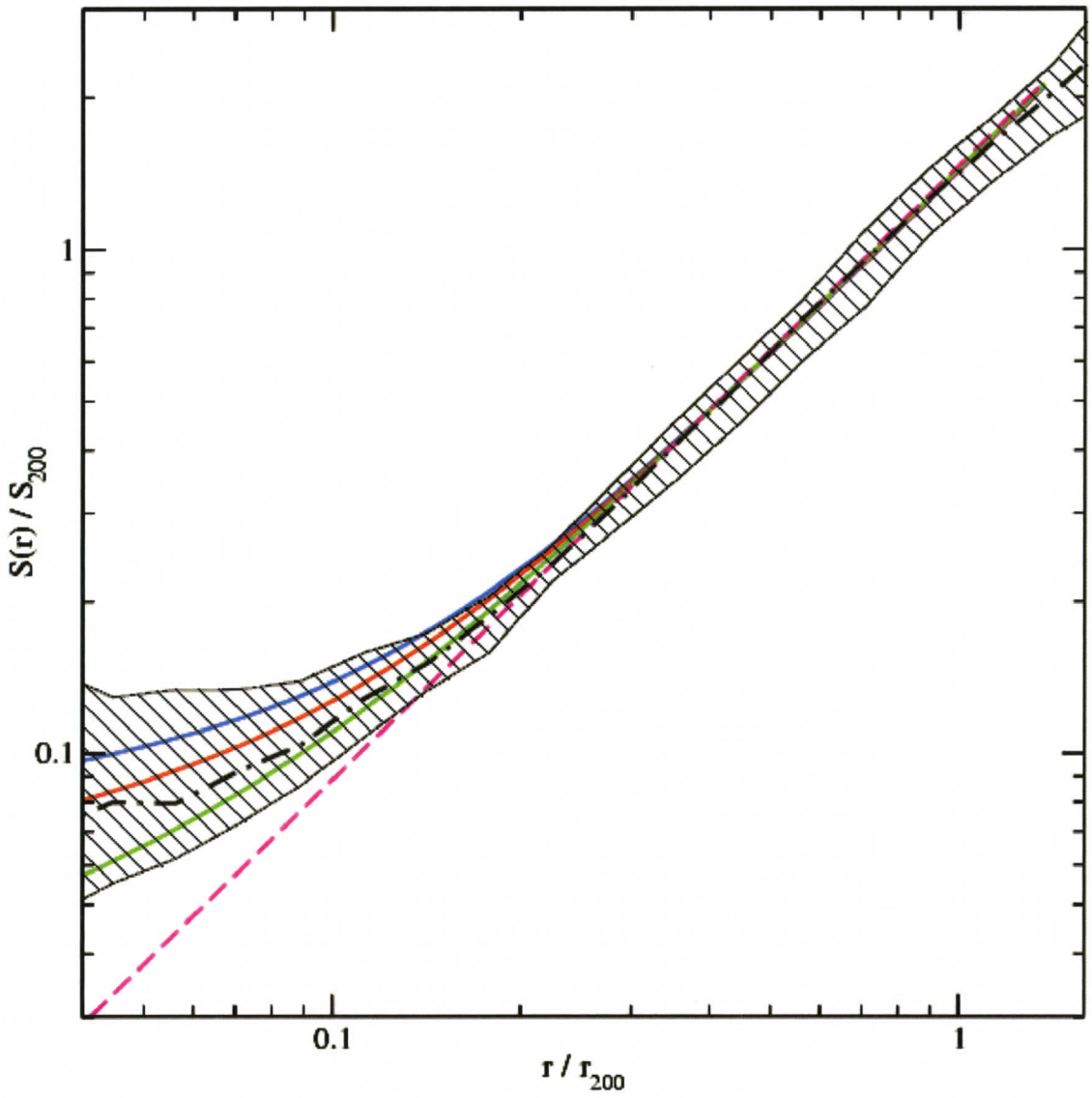

Figure 5.1: Dimensionless entropy as a function of scale radius, r/r_{200}, predicted by non-radiative cluster models with stochastically evolving substructure mass functions for a typical cluster with $M_{200} = 10^{15}\ M_{\odot}$ at $t = 5$ Gyrs. The characteristic entropy of the system, S_{200}, has a value of ≈ 2561 keV cm^2. The solid red, blue, and green curves correspond to cluster models A, B, and C, respectively. The dashed magenta line represents the initial entropy configuration of the system. The shaded region represents the entropy profiles of the simulated non-radiative clusters of Voit et al. (2005), and the dot-dashed black curve is their median entropy profile.

A comparison of the entropy profiles predicted by the non-radiative cosmological simulations of Voit et al. (2005) to those predicted by the non-radiative models with randomly evolving substructure mass functions demonstrates that the stochastic models can very well explain the scatter in the central entropies of the simulated clusters. According to Figure 5.1, the entropy profile predicted by model A is in excellent agreement with the median entropy profile of the simulated clusters. The upper level of the entropy core predicted by model B (with a shallow mass function and a large population of massive satellites) is lower than the upper core level of the simulated clusters. This is because the masses of the merging satellites in our models are mostly less than ~ 0.06 of the mass of the parent halo. The generation of very high levels of entropy cores are possibly due to major mergers with objects more massive than ~ 0.1 halo mass. The entropy distribution predicted by model C (with a steep substructure mass function and therefore, a large abundance of low-mass objects) is in a very good agreement with the lower limit of the scatter in the gas entropy predicted by the simulations.

A comparison between the non-radiative models with stochastically evolving mass functions (Figure 5.1) and those with static mass functions (Figure 4.1) demonstrates that the two models are qualitatively in agreement with each other. The entropy distribution predicted by model A and the one predicted by the static model with the mean substructure mass function (red curve in Figure 4.1) are different in the central region, with the former showing an excess entropy. This is due to the evolution of the substructure mass function in model A. The mean slope of the mass function and the corresponding cutoff mass of model A are exactly the same as the slope and the cutoff mass of the mean mass function in the static model. However, the stochastic variations of the slope (and the cutoff mass) of the evolving substructure mass function, designed to mimic the impacts of merger events and dynamical evolution of satellites, causes the difference in the final entropy configuration of the system.

The difference becomes more pronounced if we compare the entropy distribution predicted by model B to the one predicted by the static cluster model with the shallowest substructure mass function (upper blue curve in Figure 4.1). The mean slope of the evolving mass function in model B is equal to the slope of the shallowest static mass function. The cutoff mass of the static model is fixed at $M_{*,\mathrm{static}} = 0.06$, which is the highest cutoff mass that we have adopted in our cluster models (see §2). For the evolving model, on the other hand, the cutoff mass corresponding to the mean slope is set to 0.025 and its variations lie in the range $0.01 \leq M_{*,\mathrm{evolve}} \leq 0.06$. There may be massive objects falling into the cluster potential and churning up the ICM in the evolving cluster model. However, these massive satellites are not present in the ICM at all times, as opposed to the static model with the shallowest mass function. Accordingly, one expects a lower amount of heat being deposited in the ICM in the evolving model which results in lower levels of entropy core, as is seen in Figure 5.1.

The value of the core entropy predicted by model C is higher than that predicted by the static model with the steepest mass function (lower green curve in Figure 4.1). This is because the cutoff mass of the static model has a fixed value of $M_{*,\mathrm{static}} = 0.01$ (the lowest cutoff mass in our cluster models), while the cutoff mass corresponding to the mean slope in model C is set to 0.025 and its variations lie in the range $0.01 \leq M_{*,\mathrm{evolve}} \leq 0.06$, by definition. Hence, one expects a larger amount of heat being deposited in model C due to the presence of objects more massive than ≈ 0.01 of the mass of the parent halo. However, both models confirm that systems with a large abundance of low-mass subhalos are not appreciably influenced by dynamical friction heating.

According to Figure 5.1, the results of the non-radiative models with evolving substructure mass function indicate that the gas density distribution follows a power law at large radii with entropy cores present at the centre. The predictions of these models are in accordance with the results of the model with static mass functions,

suggesting that the flattening of the entropy profiles observed in cosmological simulations (Voit et al. 2005) may very well be attributable to the dynamical friction of the orbiting satellites.

5.1.2 Cluster Models with Heating and Cooling

In this section we embed our stochastic substructure mass function in cluster models that take into account the effects of radiative cooling of the gas. We study the evolution of the ICM to assess the efficiency of dynamical friction-mediated heating in clusters that are in a merger phase (with a constraint on the upper mass limit of the infalling objects such that $M_s/M_{\rm halo} \lesssim 0.06$). A comparison of the results of these models to those predicted by the model with static mass functions presented in §4.3 allows us to gauge the effects of the evolution of the mass function on the ICM. We consider the three substructure mass functions (A, B, C) discussed in §5.1.1. The initial entropy distribution is the same in all the three models and is assumed to follow the self-similar gravitational entropy profile at larger radii (equation 3.1), with isentropic cores present at smaller radii.

Plotted in Figures 5.2, 5.3, and 5.4 are the entropy profile predictions of cluster models A, B, and C, respectively, for various choices of the initial central entropies. The three systems have the same mass of $\rm M_{200} = 10^{15}\ M_{\odot}$. We start by discussing the results of model A. Figure 5.2 corresponds to model A whose mean substructure mass function is exactly the same as the static mean substructure mass function (Figure 2.4). According to the figure, systems with relatively low initial central entropies, $S_o = 10$ keV cm^2 and $S_o = 30$ keV cm^2, reach the quasi-steady state after about 1 Gyr and 2 Gyrs of radiative cooling, respectively. This is exactly similar to the corresponding results of the model with static mass function and the pure cooling model (Figures 4.2 and 4.3). These results suggest that dynamical friction heating can not offset radiative losses of the gas in cool core systems. This is because cooling scales as ${\rho_g}^2$ while dynamical friction heating scales as ρ_g. Thus,

gas cooling is dominant in central over-dense regions with low temperatures.

Increasing the initial entropy core to $S_o = 50$ keV cm$^2-$ 70 keV cm^2 results in a significant difference relative to the pure cooling model. While the pure cooling model predicts that catastrophic cooling occurs in these systems after ~ 3 Gyrs of evolution, the results of model A show that the central entropies of systems with $S_o = 50$ keV cm^2 and $S_o = 70$ keV cm^2 decline to approximately 5 keV cm^2 and 50 keV cm^2, respectively, after nearly 5 Gyrs of evolution. As the initial central densities of model clusters decrease, the gas cooling becomes less efficient and dynamical friction heating can considerably lengthen the cooling time of the gas and significantly delay the onset of the catastrophic cooling.

For a range of initial entropy levels, dynamical friction-mediated heating can completely balance radiative losses inside the cluster core. With heat deposition due to dynamical friction, the initial central entropy threshold to offset the gas cooling is, not surprisingly, lower in model A relative to the pure cooling model. According to the pure cooling model (Figure 4.2), the initial entropy level of the gas would need to be approximately $S_o \approx 300$ keV cm^2 or higher in order to ensure that the central cooling time is much longer than the age of the cluster. In model A, however, we find that in systems with mildly enhanced initial central entropies of 100 keV cm^2 $\lesssim S_o \lesssim$ 150 keV cm^2, dynamical friction heating can offset the gas cooling and maintain the thermal balance in the ICM.

For higher levels of initial entropy core, $S_o \gtrsim 200$ keV cm^2, our simplified evolving model predicts heating rates that lead to overheating of the ICM at the centre. This potentially problematic issue needs to be studied more carefully. At present, we cannot rule out the possibility that it is an outcome of our simplified treatment.

The predictions of model A are in qualitative agreement with the results of the static model studied in §5.1.2. However, there are some differences between the two models. The results of model A for initial entropy cores of $S_o = 50$ keV cm$^2 - 70$ keV cm^2 show a difference in the evolution of the gas entropy profiles

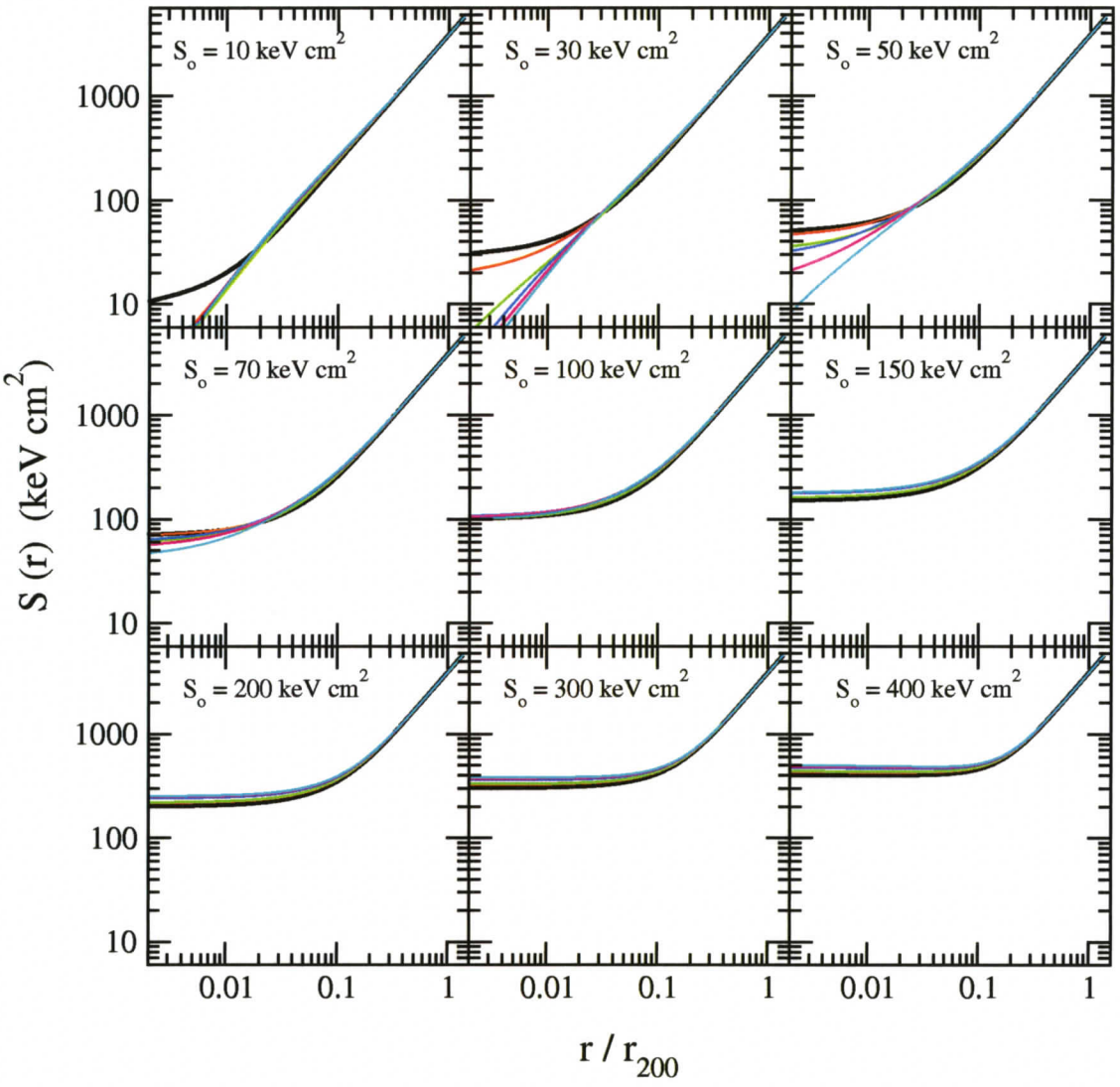

Figure 5.2: Evolution of the entropy profile predicted by model A for a typical cluster with $M_{200} = 10^{15}\ M_{\odot}$. The different panels correspond to the various levels of the core entropy. The solid black lines represent the initial entropy configuration. The red, green, blue, magenta, and cyan lines represent the entropy distribution after 1, 2, 3, 4, and 5 Gyrs of evolution, respectively.

relative to the model with static substructure mass function. According to Figure 4.3, clusters with an initial central entropy of $S_o = 50$ keV cm^2 start cooling out their entropy core after evolving for about 4 Gyrs and the central entropy of systems with $S_o = 70$ keV cm^2 drops to nearly 5 keV cm^2 after ~ 5 Gyrs. Thus the evolution of the entropy profile is slower in model clusters with stochastically evolving substructure mass functions which implies that dynamical friction heating is more efficient in these systems. As mentioned earlier, model A mimics the evolution of the substructure mass function in systems that experience mergers and in which the substructures are subject to mass loss. The variations of the slope of the mass function follow a Gaussian distribution in this model and hence the substructure mass function becomes randomly steeper and shallower than the mean mass function as it evolves with time. Since dynamical friction heating scales quadratically with substructure mass, shallower mass functions with a larger population of massive substructures contribute much more to the heating of the ICM. As a result, dynamical friction heating is more efficient in model A with randomly evolving mass functions comparing to the model with the fixed mean mass function. The minimum threshold of the initial central entropy to suppress the catastrophic cooling is lower in model A relative to the model with the static mean substructure mass function. As Figure 4.3 demonstrates, a minimum initial entropy core of $S_o = 150$ keV cm^2 is required in the static case in order to maintain the entropy floor while the corresponding value in model A is ≈ 100 keV cm^2.

Figure 5.3 presents the entropy predictions of model B. The mean substructure mass function of this model is the same as the upper scatter in the static substructure mass function (Figure 2.4). Hence the model mimics the evolution of the mass function in systems with a large population of massive substructures. Accordingly, galaxy heating is much more efficient in this model relative to model A. As the figure indicates, in systems with relatively low central entropies, 10 keV cm^2 $\lesssim S_o \lesssim$ 30 keV cm^2, dynamical friction heating fails to mitigate radiative losses, although

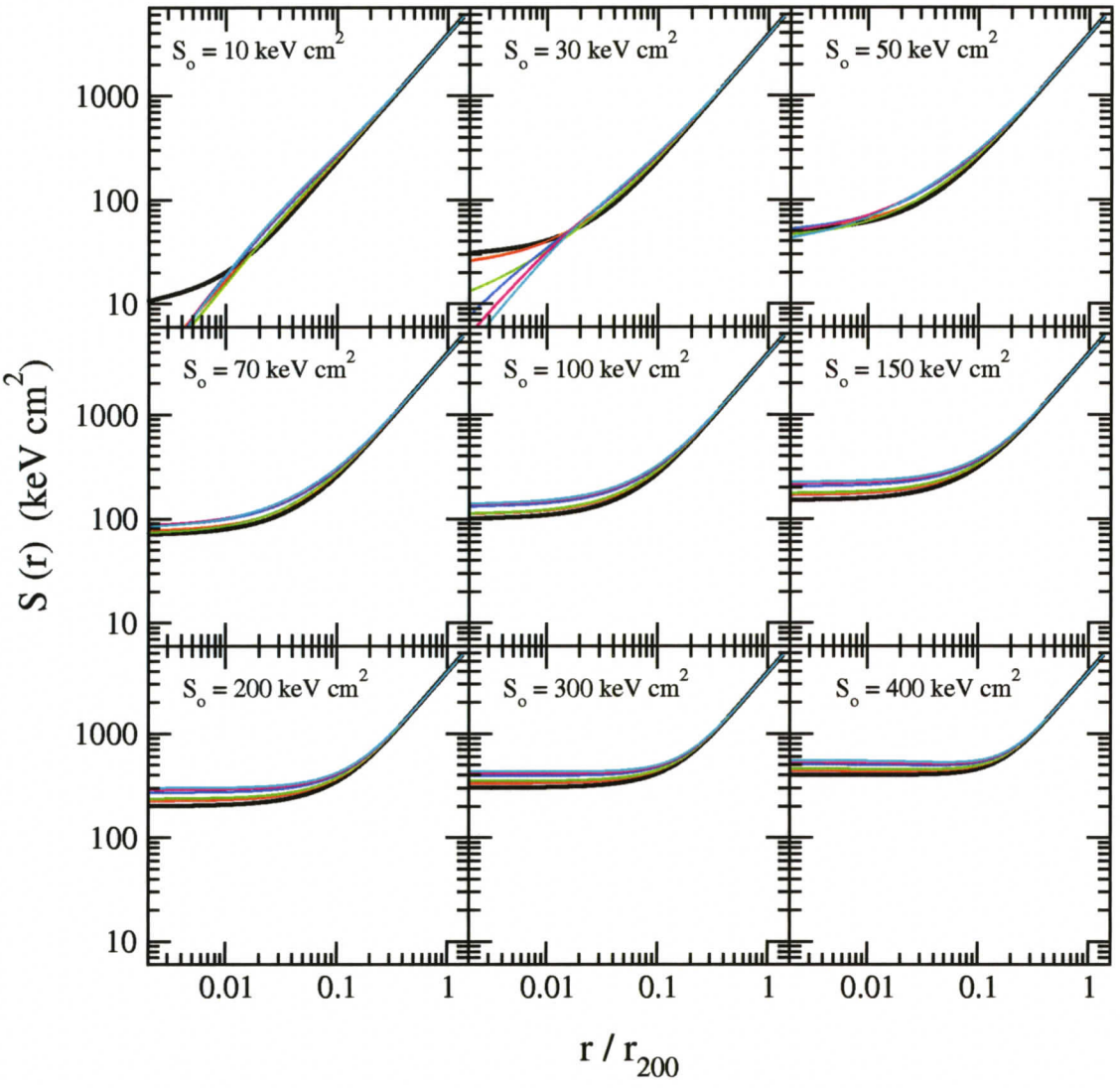

Figure 5.3: Evolution of the entropy profile predicted by model B for a typical cluster with $M_{200} = 10^{15}\ M_{\odot}$. The different panels correspond to the various levels of the core entropy. The solid black lines represent the initial entropy configuration. The red, green, blue, magenta, and cyan lines represent the entropy distribution after 1, 2, 3, 4, and 5 Gyrs of evolution, respectively.

the steady-state profiles are shallower than in model A (Figure 5.2) and in the pure cooling case (Figure 4.2).

In systems with initial entropy floor of $S_o \approx 50$ keV cm^2 galaxy stirring heating can balance radiative cooling of the central gas. The entropy threshold to achieve thermal balance in the ICM is lowered in model B due to the larger abundance of massive subhalos. This is in accordance with the predictions of the static model in §4.3, where we found that in a model cluster with a shallow substructure mass function (relative to the mean mass function; Figure 4.4), dynamical friction heating can completely forestall radiative cooling for lower initial central entropies (Figure 4.5). Increasing the initial entropy core to $S_o \gtrsim 70$ keV cm^2 results in overheating of the ICM in the central region.

Figure 5.4 shows the entropy profile predictions of model C with a mean substructure mass function that follows the lower scatter in the static mass function (Fig 2.4). The model corresponds to systems with a large abundance of low-mass substructures. Thus dynamical friction heating is less efficient in this model and one expects a higher value of minimum entropy threshold to achieve thermal balance in the ICM. As the figure indicates, dynamical friction heating is immaterial in systems with relatively low initial levels of entropy core, 10 keV cm^2 $\lesssim S_o \lesssim$ 50 keV cm^2. Cooling is dominant within the over-dense cluster core in these model clusters and galaxy stirring heating does not yield an improvement relative to the pure cooling case.

Increasing the level of the entropy core to $S_o = 70$ keV cm^2– 150 keV cm^2 results in a significant difference in evolution of the entropy profiles. The central entropy of a model cluster with $S_o = 70$ keV cm^2 drops to approximately $S_o = 5$ keV cm^2 after evolving for 5 Gyrs, whereas in the pure cooling model, a system with the same initial entropy floor starts to drop out its entropy core after ≈ 3 Gyrs. The evolution of the entropy profile becomes slower for higher levels of elevated central entropies. In a model cluster with $S_o = 150$ keV cm^2, the value of the entropy core

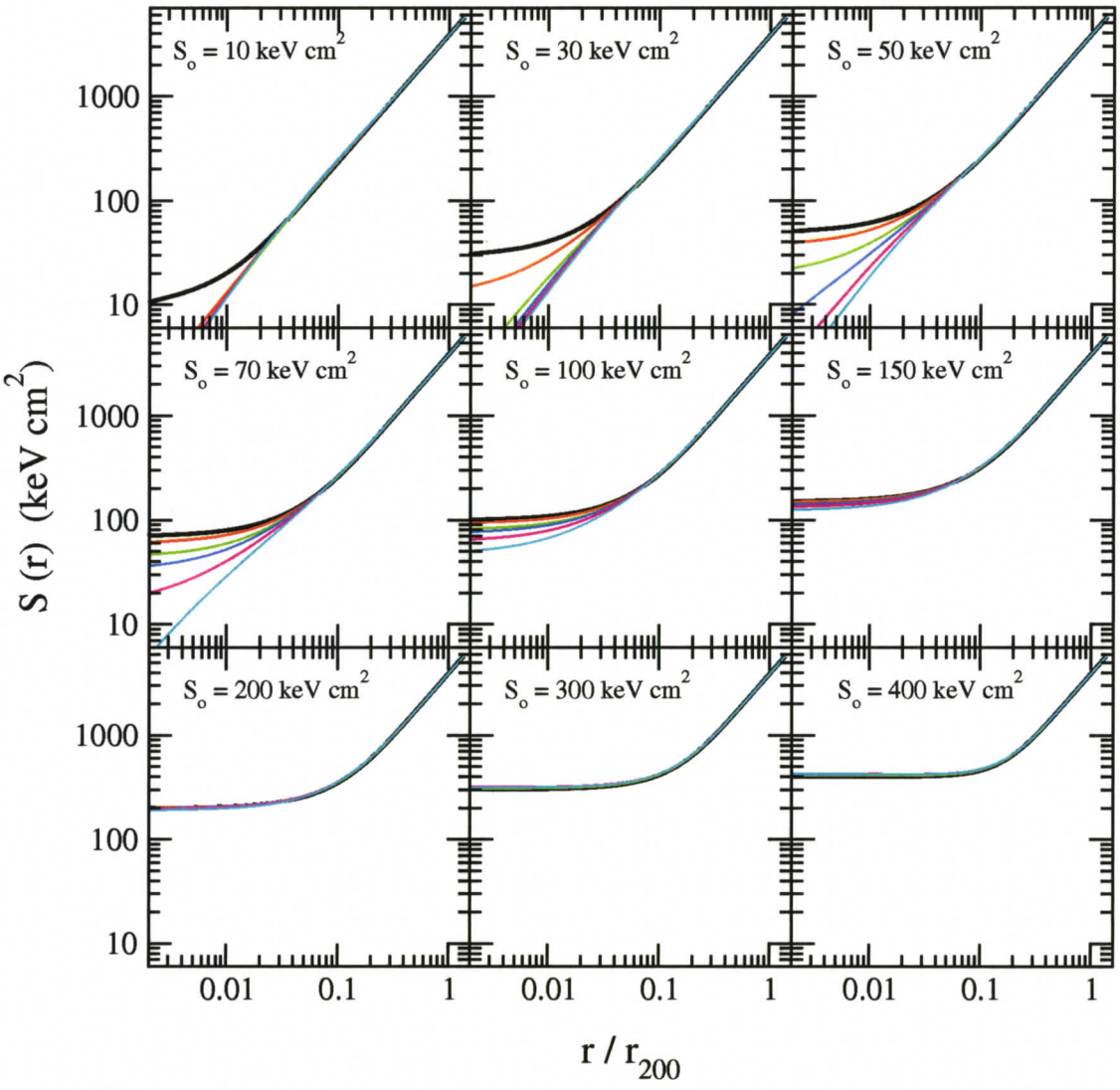

Figure 5.4: Evolution of the entropy profile predicted by model C for a typical cluster with $M_{200} = 10^{15}\ M_{\odot}$. The different panels correspond to the various levels of the initial central entropy. The solid black lines represent the initial entropy configuration. The red, green, blue, magenta, and cyan lines represent the entropy distribution after 1, 2, 3, 4, and 5 Gyrs of evolution, respectively.

declines to nearly 110 keV cm^2 after 5 Gyrs, whereas the corresponding value for the pure cooling model is approximately 30 keV cm^2. Thus, the role of dynamical friction heating in moderating the radiative losses is still apparent in systems with a lower abundances of massive substructures, if the systems have sufficiently enhanced central entropies.

In the presence of higher entropy cores, S_o = 250 keV cm^2– 400 keV cm^2, galaxy stirring heating can completely balance the radiative losses of the gas at the centre. Although the role of dynamical friction heating in delaying the onset of catastrophic cooling is apparent in model C, the efficiency of the dynamical friction of the moving satellites is lower in this model relative to models A and B due to the lower abundance of massive satellites in this model.

5.2 Clusters in Post-Merger Phase

In the previous section we studied the impacts of the evolution of the substructure mass function on the ICM in clusters that are actively gaining mass through merging. As mentioned earlier, some clusters are in post-merger phase, where the injection of satellites has tapered off. Hence the evolution of the substructure mass function in these systems is governed by the orbital decay of cluster members. The substructure mass function steepens due to mass loss of satellite galaxies through tidal stripping and gravitational shocks as they orbit inside the cluster halo (Taylor & Babul, paper I). Since dynamical friction heating scales as the square of substructure mass, $M_s{}^2$, one expects it to become less efficient at late times as the mass function steepens and the massive substructures lose mass.

A proper model for the evolution of the substructure mass function in systems that are in post-merger phase requires detailed analysis of the dynamical evolution of the cluster members. This is beyond the scope of this work. Similar to the case of clusters with randomly evolving substructure mass functions, here we attempt

to develop a simple scheme to model the evolution of the mass function in these systems by drawing upon the semi-analytic model of halo formation of Benson et al. (2002a,b, 2003). We find that for 5 systems in our sample of 20 realization of the merger tree, the substructure mass function decays smoothly with time. When we plot up the entire spread of the mass function for the 5 sample clusters at different time steps, we find that the upper and lower mass functions of the set roughly lie between the static mean mass function and its lower scatter that we fit in §2 (Figure 2.4). Accordingly, we assume that the initial substructure mass function of the model cluster initially follows the mean mass function in the static model and that it decays smoothly to the lower scatter in the static mass function after evolving for nearly 5 Gyrs. The rate of the decay of the mass function depends on the evolution of substructures orbiting in the potential of the main halo and may vary from one system to another. Based on our sample of 5 clusters, we find that a linear correlation between the age of the system and the slope of the substructure mass function matches the evolutionary trend relatively well. The correlation is defined as $\alpha \approx 0.01\ (t/\mathrm{Gyr}) + \alpha_m$, where α_m is the low-mass-end slope of the (static) mean mass function and t is the age of the system. However, a sample of 5 clusters is not a statistically sound basis to derive this correlation. We leave the accurate analysis of the smooth decay of the substructure mass function for future work.

The initial entropy configuration of the cluster model with smoothly evolving mass function is assumed to follow the self-similar gravitational entropy profile at large radii (equation 3.1) with isentropic cores at small radii. Plotted in Figure 5.5 are the entropy profile predictions of this simple cluster model for various choices of the initial central entropies. According to the figure, dynamical friction heating is immaterial in systems with an initial entropy core of $S_o \lesssim 70$ keV cm^2. Cooling is dominant inside the over-dense cluster core and galaxy stirring heating does not yield an improvement relative to the pure cooling case.

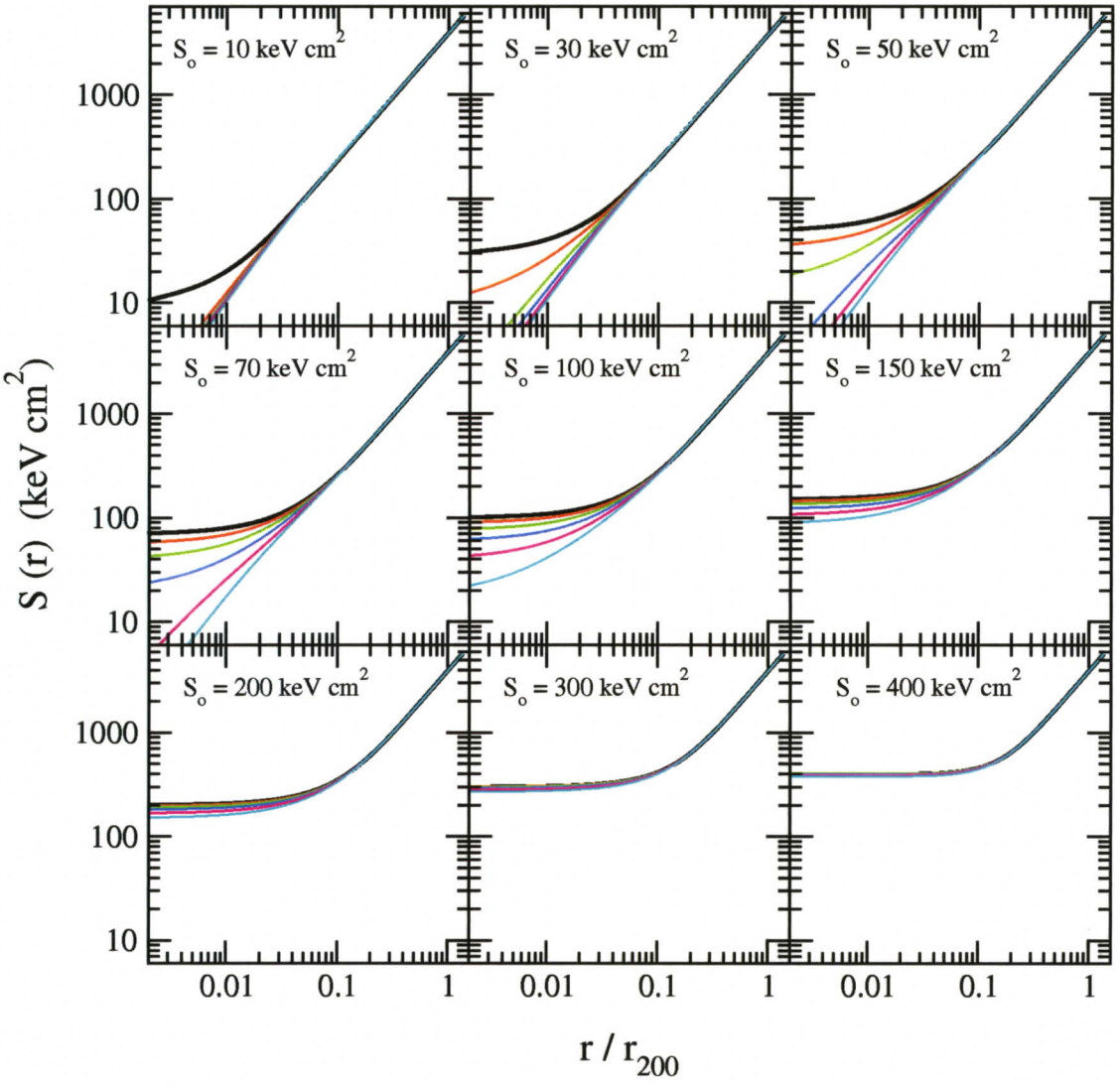

Figure 5.5: Evolution of the entropy profile predicted by the dynamical heating + cooling model with smoothly evolving substructure mass functions for a cluster with $M_{200} = 10^{15}\ M_{\odot}$. The different panels correspond to the various levels of the core entropy. The solid black lines represent the initial entropy configuration. The red, green, blue, magenta, and cyan lines represent the entropy distribution after 1, 2, 3, 4, and 5 Gyrs of evolution, respectively.

The central entropy of model clusters with $S_o = 100$ and 150 keV cm^2 decreases to approximately 20 and 90 keV cm^2, respectively, after nearly 5 Gyrs of evolution. In the pure cooling model, on the other hand, clusters with $S_o = 100$ keV cm^2 start to drop out their entropy core after cooling for ≈ 4 Gyrs and the central entropy of clusters with $S_o = 150$ keV cm^2 drops to nearly 25 keV cm^2 after about 5 Gyrs. Hence, increasing the level of the initial entropy core results in a significant difference in the evolution of the gas entropy distribution relative to the pure cooling case. This is in agreement with the results of the models with static (§ 4.3) and stochastically evolving (§ 5.1.2) mass function. The role of galaxy stirring becomes more pronounced in clusters with relatively higher levels of initial entropy core because gas cooling becomes much less efficient in high temperature under-dense regions. The minimum threshold of the initial central entropy to balance the radiative losses inside the cluster core is approximately 300 keV cm^2 in this model.

Although the role of dynamical friction heating in moderating radiative cooling is apparent in the model with smoothly decaying substructure mass function, the efficiency of galaxy stirring is lower, as expected, in this case relative to the models with stochastically evolving mass functions and the static model. This is because of the low abundance of massive objects at late times due to their mass loss. As a result, radiative losses would become increasingly dominant as the systems evolve with time.

5.3 Summary

Based on the results of models A, B, and C with stochastically evolving substructure mass functions and the cluster model with smoothly evolving mass function, we conclude that dynamical friction heating is an important reservoir of energy in the ICM; it can mitigate the radiative losses inside the cooling region and significantly delay the onset of catastrophic cooling. The predictions of the models are in rea-

sonable agreement with the results of the cluster models with static mass function discussed in §4.3. They confirm that galaxy heating is immaterial in clusters that start out in a cool core configuration and that dynamical friction-induced heating can suppress radiative cooling in systems that have experienced sufficient amount of entropy injection.

Chapter 6

Summary & Discussions

Cluster galaxies lose energy due to the process of dynamical friction as they orbit through the cluster halo. In principle, the kinetic energy in the orbital motions of galaxies is sufficient to offset the radiative cooling losses of the gas if the kinetic energy can be converted into thermal energy with sufficiently high efficiency (e.g., Miller 1986; El-Zant et al. 2004; Kim et al. 2005). In this dissertation, we explore in detail the role of dynamical friction-mediated heating on the evolution of the ICM. We derive the local heating flux assuming that the induced heat is deposited locally at the location of galaxies (equation 3.9). We consider two different models with static (§ 4) and evolving (§ 5) substructure mass functions. For the latter case, we consider systems that are in a merger phase and have randomly evolving mass functions (§5.1), and systems that are in a post-merger phase and whose mass functions steepen smoothly with time due to mass loss (§5.2). We study the influences of galaxy stirring heating on the evolution of the ICM in both non-radiative clusters (where radiative cooling is not taken into account, §§ 4.1 and 5.1.1) and clusters where radiative losses are present and compete with galaxy heating to shape the properties of the system (§§ 4.3, 5.1.2, and 5.2).

The results of non-radiative cluster models suggest that dynamical friction of orbiting substructures is responsible for the flattening of self-similar gravitational entropy profiles inside the cluster core. The generation of near-isentropic entropy cores with a large distribution in their values was originally observed in recent high-resolution non-radiative cosmological simulations of galaxy clusters (Voit et

al. 2005) and to date, no clear explanation for this feature has been forthcoming. The degree of the flattening of the entropy profiles in our non-radiative models demonstrates the efficacy of dynamical friction heating. Both models with static and randomly evolving substructure mass functions recover very well the spread in the central entropies observed in non-radiative simulated clusters. The level of the generated entropy core is higher in systems with a large population of massive substructures and lower in clusters with a large abundance of low-mass subhalos (Figure 4.1 and 5.1).

The results of cluster models with radiative cooling of the gaseous component imply that galaxy stirring heating can not be the only heating mechanism in the ICM. If systems start out in a cool core configuration, with their initial entropy profiles following the self-similar gravitational profile, dynamical friction-induced heating can not prevent or delay the onset of catastrophic cooling. This is because radiative cooling scales as the square of gas density, while dynamical friction heating scales linearly with the density. Hence gas cooling is dominant inside the over-dense central regions in these systems and it eventually leads to a cooling catastrophe. The situation is improved if the clusters have experienced entropy injection to warm or hot cores, because radiative cooling becomes much less efficient in high temperature under-dense regions. We find that in systems with sufficient amount of entropy injection, dynamical friction heating can efficiently mitigate radiative losses of the gas at the centre and delay (or in some cases prevent) the onset of catastrophic cooling. These models provide a viable explanation for the observed profiles of CWC clusters with short central cooling times, yet no evidence for recent AGN activities (Donahue et al. 2005).

One possible interpretation of such systems is that the intracluster gas has experienced an unusually strong AGN outburst approximately 1 Gyr in the past, with 1 Gyr being the usual estimate of core cooling time of the gas in these systems. In fact, if these systems have been cooling for 1 Gyr and presently have core entropies

of 30−50 keV cm^2, they must have been heated to 55−75 keV cm^2 initially. The required AGN energy to raise the gas entropy to the observed level is 3.0−4.7 $\times$ 10^{62} ergs, which is among the strongest and rarest bursts in comparison to typical outflow energies (Donahue et al. 2005). These estimates, however, ignore the effects of galaxy stirring. Taking into account galaxy stirring heating and the fact that clusters are still accreting mass, we find that the required outburst energy, if the burst occurred $\sim$ 1 Gyr ago, is reduced to 1.3−3.3 $\times$ 10^{62} ergs. Although the energy requirements are lowered by a factor of $\sim$ 2−3 relative to the case with no galaxy stirring, they are still higher than the typical AGN energy output. The energetics can be even lowered to $\approx$ 6 $\times$ 10^{61} ergs in systems with a large population of massive subhalos. This is comparable to the outflow energies of the most powerful AGN bursts discovered to date in Hercules A (Nulsen et al. 2005) and MS0735.6+7421 (McNamara et al. 2005). However, these systems appear to be rare at the present time.

As the amount of the injected energy increases and radiative cooling becomes less efficient, galaxy heating can substantially decrease the cooling rate of the gas. According to Figure 4.3, for S_o = 55 keV cm^2 and 70 keV cm^2, the central entropy of the model clusters that take into account galaxy heating reduces to approximately 30 keV cm^2 and 50 keV cm^2, respectively, after evolving for $\sim$ 2 Gyrs. Comparing to the pure cooling case, we find that dynamical friction heating more than doubles the central cooling time of the gas in these systems. Hence it is possible that the central gas in the observed CWC clusters experienced an extreme AGN burst $\gtrsim$ 2 Gyrs ago and dynamical friction heating have churned up the ICM and slowed down gas cooling since then. The AGN outburst can be delayed to earlier times ($\gtrsim$ 3 Gyrs) in systems with a very large abundance of massive subhalos wherein galaxy heating is more efficient.

An alternative model is the one in which the central gas is pre-heated through early episodes of entropy injection (e.g. AGN) before it becomes a constituent

of the virialized cluster environment (Evrard & Henry 1991; Kaiser 1991; Bower 1997; Balogh et al. 1999; Babul et al. 2002; Voit et al. 2002; Oh & Benson 2003; McCarthy et al. 2004, 2008). An important feature of the pre-heating model is that the energy requirements to reach the observed cluster's present configurations can be potentially lowered relative to the models with present-day internal heating. The results of the dynamical friction heating + cooling model with static substructure mass function (Figure 4.3) demonstrate that the central entropies of clusters with pre-heating levels of $S_o = 85{-}100$ keV cm^2 decline to $30{-}50$ keV cm^2 after evolving for approximately 5 Gyrs, which is the typical age of massive clusters. If pre-heating occurs at $1< z <2$, the total energy required to elevate the central entropy of the gas to $S_o = 85{-}100$ keV cm^2 ranges between $4{-}5 \times 10^{60}$ ergs, which is approximately two order of magnitudes less energy than if the clusters were heated from within at the present epoch (McCarthy et al. 2008). This is because the mean baryon density is much lower at z 1$\sim$2 relative to the present-day mean baryon density and therefore, much less energy is required to elevate the entropy of the gas to the desired level. The pre-heating energetics can be reduced to $2{-}2.5 \times 10^{60}$ ergs (corresponding to pre-heating levels of $40{-}50$ keV cm^2) in cluster halos that host a large population of massive subhalos (Figure 4.5 and 5.3).

In the context of the pre-heating model, it is possible that the central gas in the observed clusters Abell 1650 and Abell 2244 is pre-heated to $S_o \sim 80{-}100$ keV cm^2 and the systems have evolved following the combined action of cooling and galaxy stirring heating since then. In this scenario, the central gas has not yet cooled to the point at which it can trigger the central black hole into action. Although galaxy stirring can efficiently slow down radiative cooling, the tendency of these models is to evolve towards the pure cooling configuration. If the model continues to evolve, the gas will eventually cool, flow inward, and accrete onto the central black hole. This triggers an AGN outburst which will then heat up the surrounding medium and forestall further inflow of matter (McCarthy et al. 2008). Therefore,

a prediction of the model is that clusters with relatively mild pre-heating levels ($\sim$ 70$-$100 keV cm^2) transform slowly into systems that resemble the observed CWC clusters and will eventually evolve into systems that resemble the CCC clusters.

Figure 4.2 shows that pre-heating the pure cooling model to S_o = 150$-$180 keV cm^2 and evolving it for nearly 5 Gyrs results in entropy profiles that are in agreement with the observed profiles of the two CWC systems. A comparison of the predictions of the dynamical friction heating + cooling model to the results of the pure cooling model demonstrates that the pre-heating levels required to match the observed entropy profiles are lower in the former case by a factor of $\sim$ 2.

In the dynamical friction heating + cooling models (with static and varying substructure mass functions), galaxy heating can completely balance radiative losses for range of pre-heating levels, $S_o \approx$ 100$-$200 keV cm^2 (with $S_o \sim$ 150 keV cm^2 corresponding to the model with the static mean mass function). The minimum threshold of entropy in the pure cooling model in order to ensure that the central cooling time is long compared to the age of the cluster is approximately 300 keV cm^2. Hence energetics of pre-heating can be reduced due to heat deposition through galaxy stirring.

Chapter 7 | *Conclusions*

In this work we examine the effects of dynamical friction heating on the thermal evolution of the ICM. To assess these effects, we develop a 1-D model for the ICM that accounts for dynamical friction of the orbiting satellite galaxies. We investigate entropy evolution of non-radiative clusters and clusters where radiative losses compete with galaxy heating to shape the structure of the ICM. The main results can be summarized as follows:

- Dynamical friction of galaxies can generate entropy cores in non-radiative clusters. This can explain the observed flattening of self-similar entropy profiles inside the core of non-radiative simulated cluster of Voit et al. (2005). The diversity in the value of the central entropy of our non-radiative clusters is in very good agreement with that predicted by cosmological simulations.

- Dynamical friction-mediated heating can not be the only heating mechanism in galaxy clusters. Dynamical friction heating is immaterial in systems that are in cool core configuration with no other heating mechanisms operating in the ICM; it can not counteract radiative losses and account for the observed properties of galaxy clusters.

- The situation is completely different if the systems have experienced a sufficient amount of entropy injection through pre-heating or possibly some form of present-day internal heating (e.g. AGN outbursts). In this case, dynamical friction heating can substantially alter the rate at which the gas cools down.

- In the context of the dynamical friction-heating + cooling models, we study the observations of the two warm core clusters with short central cooling times, but no evidence for recent or ongoing AGN activities (Donahue et al. 2005). We investigate different scenarios that can explain the observed profiles of these systems. We find that:

  - The clusters may be heated internally through a very strong AGN outburst. Taking to account the effects of galaxy heating, the energy requirements of the outburst can be lowered by a factor of 2, if the burst occurred $\sim$ 1 Gyr in the past, or it can push the AGN outburst further back to $\gtrsim$ 2 Gyrs.

  - An alternative interpretation is that the systems are pre-heated to mild levels of $\sim$ 70$-$100 keV cm^2 and dynamical friction heating has slowed down the radiative losses such that the central gas has never cooled to the point at which it can trigger an AGN outburst.

Bibliography

The following abbreviations are used in this bibliography:

MNRAS: Monthly Notices of the Royal Astronomical Society

ApJ: The Astrophysical Journal

ApJ: The Astrophysical Journal Letters

ApJSS: The Astrophysical Journal Supplement Series

AJ: The Astronomical Journal

A&A: Astronomy and Astrophysics

Ap&SS: Astrophysics and Space Science

ARA&A: Annual Reviews of Astronomy and Astrophysics

PASP: Proceedings from the Astronomical Society of the Pacific

PhST: Physica Scripta volume T

CoASP: Comments on Astrophysics and Space Physics

NewAR: New Astronomy Reviews

Allen S. W., Schmidt R. W., Fabian A. C. **2002**, MNRAS, 334, L11

Allen S. W., Schmidt R. W., Ebeling H., Fabian A. C. **2004**, A&A, 441, 893

Arnaud M., Pointecouteau E., Pratt G. W. **2005**, MNRAS, 353, 457

Babul A., Balogh M. L., Lewis G.F., Poole G. B. **2002**, MNRAS, 330, 329

Balogh M. L., Babul A., Patton D. R. **1999**, MNRAS, 307, 463

Balogh M. L., Pearce F. R., Bower R. G., Kay S. T. **2001**, MNRAS, 326, 1228

Benson A. J., Bower R. G., Frenk C. S., Lacey C. G., Baugh C. M., Cole S. **2003**, ApJ, 599, 38

Benson A. J., Lacey C. G., Baugh C. M., Cole S., Frenk C. S. **2002a**, MNRAS, 333, 156

Benson A. J., Frenk C. S., Lacey C. G., Baugh C. M., Cole S. **2002b**, MNRAS, 333, 177

Bildfell C., Hoekstra H., Babul A., Mahdavi A. **2008**, astro-ph/0802.2712

Binney J., Tabor G. **1995**, MNRAS, 276, 663

Bondi H., Hoyle F. **1944**, MNRAS, 104, 273

Bower R. G. **1997**, MNRAS, 288, 355

Brighenti F., Mathews W. G. **2006**, ApJ, 643, 120

Burles S., Nollett K. M., Turner M. S. **2001**, ApJ, 552, L1

Carlberg R. G., Yee H. K. C., Ellingson E. **1997**, ApJ, 478, 462

Carlstrom J. E., Holder G. P., Reese E. D. **2002**, ARA&A, 40, 643

Chandrasekhar S. **1943**, ApJ, 97, 255

Churazov E., Brüggen M., Kaiser C. R., Böhringer H., Forman W. **2001**, ApJ, 554, 261

Cohn J. D., White M. **2005**, Astroparticle Physics, 24, 316

Conroy C., Ostriker J. P. **2008**, astro-ph/0712.0824

Crain R. A., Eke V. R., Frenk C. S., Jenkins A., McCarthy I. G., Navarro J. F., Pearce F. R. **2007**, ApJ, 377, 41

Davé R., Katz N., Weinberg D. H. **2006**, ApJ, 579, 23

De Grandi S., Molendi S. **2002**, 567, 163

Donahue M., Horner D. J., Cavagnolo K. W., Voit G. M. **2006**, ApJ, 643, 730

Donahue M., Voit G. M., O'Dea C. P., Baum S. A., Sparks W. B. **2005**, ApJ, 630, L13

El-Zant A. A., Kim W.-T., Kamionkowski M. **2004**, MNRAS, 354, 169

Ettori S. **2003**, MNRAS, 344, L13

Evrard A. E., Henry J. P. **1991**, ApJ, 383, 95

Evrard A. E., Metzler C. A., Navarro J. F. **1996**, ApJ, 469, 494

Fabian A. C. **1994**, ARA&A, 32, 277

Faltenbacher A., Kravtsov A. V., Nagai D., Gottlöber S. **2005**, MNRAS, 358, 139

Frenk C. S., White S. D. M., Bode P., Bond J. R., Bryan G. L., Cen R., Couchman H. M. P., Evrard A. E., Gnedin N., Jenkins A., Khokhlov A. M., Klypin A., Navarro J. F., Norman M. L., Ostriker J. P., Owen J. M., Pearce F. R., Pen U.-L., Steinmetz M., Thomas P. A., Villumsen J. V., Wadsley J. W., Warren M. S., Xu G., Yepes G. **1999**, ApJ, 525, 554

Gao L., White S. D. M., Jenkins A., Stoehr F., Springel V. **2004**, MNRAS, 355, 819

Hoekstra H., Franx M., Kuijken K., Squires G. **1998**, ApJ, 504, 636

Hoekstra H., Mellier Y., van Waerbeke L., Semboloni E., Fu L., Hudson M. J., Parker L. C., Tereno I., Benabed K. **1998**, ApJ, 647, 116

Holder G. P., Mohr J. J., Carlstrom J. E., Evrard A. E., Leitch E. M. **1998**, ApJ, 544, 629

Holder G. P., McCarthy I. G., Babul A. **1998**, MNRAS, 382, 1697

Kaiser N. **1991**, ApJ, 383, 104

Kang X., Jing Y. P., Mo H. J., Börner G. **2005**, ApJ, 631, 21

Kay S. T., Thomas P. A., Jenkins A., Pearce F. R. **2004**, MNRAS, 355, 1091

Kim W.-T., El-Zant A. A., Kamionkowski M. **2005**, ApJ, 632, 157

Kim H., Kim W.-T. **2007**, ApJ, 665, 432

Kosowsky A. **2006**, NewAR, 50, 969

Lea S. M., De Young D. S. **1976**, ApJ, 210, 647

Lewis G. F., Babul A., Katz N., Quinn T., Hernquist L., Weinberg D. H. **2000**, ApJ, 536, 623

Lin Y.-T., Mohr J. J., Stanford S. A. **2003**, ApJ, 591, 749

Mahdavi A., Hoekstra H., Babul A., Sievers J., Myers S. T., Henry J. P. **2007**, ApJ, 664, 162

Mather J. C., Cheng E. S., Eplee Jr. R. E., Isaacman R. B., Meyer S. S., Shafer R. A., Weiss R., Wright E. L., Bennett C. L., Boggess N. W., Dwek E., Gulkis S., Hauser M. G., Janssen M., Kelsall T., Lubin P. M., Moseley Jr. S. H., Murdock T. L., Silverberg R. F., Smoot G. F., Wilkinson D. T. **1990**, ApJ, 354, L37

Mathews W. G., Brighenti F., Buote D. A. **2004**, ApJ, 615, 662

McCarthy I. G., Babul A., Bower R. G., Balogh M. L. **2008**, MNRAS, 386, 1309

McCarthy I. G., Bower R. G., Balogh M. L. **2007**, MNRAS, 377, 1457

McCarthy I. G., Balogh M. L., Babul A., Poole G. B., Horner D. J. **2004**, ApJ, 613, 811

McNamara B. R., Nulsen P. E. J., Wise M. W., Rafferty D. A., Carilli C., Sarazin C. L., Blanton E. L. **2005**, Nature, 433, 45

Mellier Y. **1999**, ARA&A, 37, 127

Miller L. **1986**, MNRAS, 220, 713

Muchovej S., Mroczkowski T., Carlstrom J. E., Cartwright J., Greer C., Hennessy R., Loh M., Pryke C., Reddall B., Runyan M., Sharp M., Hawkins D., Lamb J. W., Woody D., Joy M., Leitch E. M., Miller A. D. **2007**, ApJ, 663, 708

Navarro J. F., Frenk C. S., White S. D. M. **1997**, ApJ, 490, 493

Neto A. F., Gao L., Bett P., Cole S., Navarro J. F. Frenk C. S., White S. D. M., Springel V., Jenkins A. **2007**, MNRAS, 381, 1450

Nulsen P. E. J., Hambrick D. C., McNamara B. R., Rafferty D., Birzan L., Wise M. W., David L. P. **2005**, ApJ, 625, L9

Nusser A., Silk J., Babul A. **2006**, MNRAS, 373, 739

Oh S. P., Benson A. J. **2003**, MNRAS, 342, 664

Peterson J. R., Kahn S. M., Paerels F. B. S., Kaastra J. S., Tamura T., Bleeker J. A. M., Ferrigno C., Jernigan J. G. **2003**, ApJ, 590, 207

Peterson J. R., Paerels F. B. S., Kaastra J. S., Arnaud M., Reiprich T. H., Fabian A. C. Mushotzky R. F., Jernigan J. G., Sakelliou I. **2001**, A&ApJ, 365, L104

Piffaretti R., Jetzer P., Kaastra J. S., Tamura T. **2005**, A&A, 433, 101

Poole G. B., Babul A., McCarthy I. G., Sanderson A. J. R., Fardal M. A. **2008**, astro-ph/0804.1552

Pratt G. W., Arnaud M., Pointecouteau E. **2006**, A&A, 446, 429

Pratt G. W., Böhringer H., Croston J. H., Arnaud, M., Borgani S., Finoguenov A., Temple R. F. **2007**, A&A, 461, 71

Raymond J. C., Smith B. W. **1977**, ApJS, 35, 419

Rephaeli Y., Salpeter E. E. **1980**, ApJ, 240, 20

Ruhl J., Ade P. A. R., Carlstrom J. E., Cho H.-M., Crawford T., Dobbs M., Greer C. H., Halverson N. w., Holzapfel W. L., Lanting T. M., Lee A. T., Leitch E. M., Leong J., Lu W., Lueker M., Mehl J., Meyer S. S., Mohr J. J., Padin S., Plagge T., Pryke C., Runyan M. C., Schwan D., Sharp M. K., Spieler H., Staniszewski Z., Stark A. A. **2004**, Society of Photo-Optical Instrumentation Engineers (SPIE) , pp 11-29

Sanderson A. J. R., Ponman T. J., O'SullivanE. **2006**, MNRAS, 372, 1496

Sarazin C. L. **1988**, *X-ray Emission from Clusters of Galaxies*, Cambrdige University Press

Schipper L. **1974**, MNRAS, 168, 21

Spergel D. N., Verde L., Peiris H. V., Komatsu E., Nolta M. R., Bennett C. L., Halpern M., Hinshaw G., Jarosik N., Kogut A., Limon M., Meyer S. S., Page L., Tucker G. S., Weiland J. L., Wollack E., Wright E. L. **2003**, ApJSS, 148, 175

Sunyaev R. A., Zeldovich Y. B. **1970**, Ap&SS, 7, 3

Sunyaev R. A., Zeldovich Y. B. **1970**, CoASP, 4, 173

Taylor J. E., Babul A. **2001**, ApJ, 559, 716

Taylor J. E., Babul A. **2004**, MNRAS, 348, 811

Taylor J. E., Babul A. **2005**, MNRAS, 364, 515

Taylor J. E., Babul A. **2005**, MNRAS, 346, 535

Vale A., Ostriker J. P. **2006**, MNRAS, 371, 1173

Vikhlinin A., Kravtsov A., Forman W., Jones C., Markevitch M., Murray S. S., Van Speybroeck L. **2006**, ApJ, 640, 691

Voit G. M., Bryan G. L., Balogh M. L., Bower R. G. **2002**, ApJ, 576, 601

Voit G. M., Donahue M. **2005**, ApJ, 634, 955

Voit G. M., Kay S. T., Bryan G. L. **2005**, MNRAS, 364, 909

White S. D. M., Navarro J. F., Evrard A. E., Frenk C. S. **1993**, Nature, 366, 429